TIGHT-BINDING CALCULATION OF ELECTRONIC PROPERTIES OF OLIGOPHENYL AND OLIGOACENE NANORIBBONS

A THESIS

SUBMITTED TO THE GRADUATE SCHOOL

IN PARTIAL FULFILLMENT OF THE REQUIREMENTS

FOR THE DEGREE

MASTER OF SCIENCE

BY

ADAM HINKLE

CO-ADVISORS: ANTONIO C. CANCIO AND MAHFUZA KHATUN

BALL STATE UNIVERSITY

MUNCIE, INDIANA

JULY 2008

To the memory of my mother,

with love and gratitude

Abstract

Tight-Binding Calculation of Electronic Properties of Oligophenyl and Oligoacene nanoribbons.

Within recent years, allotropic structures of carbon have been produced in the forms of tubes and ribbons which offer the promise of extraordinary electronic and thermal properties. Here we present analyses of oligophenyl and oligoacene systems–infinite, one-dimensional chains of benzene rings linked along the armchair and zigzag directions. These one-dimensional structures, which are amenable to calculation by analytical means, exhibit features very similar to carbon nanotubes and nanoribbons. Using a tight-binding Hamiltonian we analytically determine the density of states, local density of states, and energy-band structure for the phenyl and the acene. We also examine the effect of disorder on the energies and the corresponding states.

Isn't it enough to see that a garden is beautiful without having to believe that there are fairies at the bottom of it too?

Douglas Adams

Contents

Acknowledgments **viii**

1 Introduction **1**

1.1 Nanoscience 1

1.2 Motivation for the Study 2

1.2.1 Introduction 2

1.2.2 Carbon Nanotubes 3

1.2.3 Nanoribbons and Nanostrips 4

1.3 Tight-Binding Overview 5

1.4 The Thesis Work 6

1.5 Preview 7

2 The Tight-Binding Model **8**

2.1 Synopsis 8

2.2 Benzene (Neglecting the Hydrogen) 9

2.3 Tight-binding Formalism and Benzene 13

3 Oligophenyl **19**

3.1 Unperturbed Oligophenyl 19

3.1.1 Introduction 19

3.1.2 Energy and Density of States 20
3.1.3 Symmetries and Edge States 22
3.2 Perturbed Oligophenyl 24
3.2.1 Introduction 24
3.2.2 Perturbing the Oligophenyl 24
3.2.3 Local Density of States 27

4 Oligoacene **34**
4.1 Unperturbed Oligoacene 34
4.1.1 Introduction 34
4.1.2 Energy and Density of States 35
4.2 Perturbed Oligoacene 38
4.2.1 Energy Bands and Density of States 38
4.2.2 LDOS 41

5 Summary and Conclusions **47**

A Sample Python Codes **50**
A.1 Scripting for Generating the Hamiltonian 51
A.2 Density of States 52
A.3 Local Density of States 54

B Additional Matrix-Hamiltonian Scripts **56**

Bibliography **59**

List of Figures

1.1 The manner in which a graphene sheet is wrapped is represented by a pair of integer-indices, (n, m), which denote a chiral vector, $\vec{C}$, or chirality of the structure. If $m = 0$, the configuration is "zigzag." If $n = m$, the configuration is "armchair." For all other cases, it is simply chiral. The vector, $\vec{T}$, runs along the length of the tube. The tube is folded in such a way that connecting the point described by $\vec{C}$ to its origin constructs a seamless cylinder. 3

1.2 Armchair (left) and zigzag nanoribbons (right) [1]. The vector $\vec{L}$ runs along the length of the ribbon, while vector $\vec{T}$ defines the ribbon's width. 4

2.1 The benzene molecule has six carbon atoms (black) bonded together in the hexagonal shape with an outer ring of hydrogen atoms (white) bonded to each carbon. The repeating unit-cell (used in Section 2.3) is highlighted by the dashed lines and consists of one carbon atom and one hydrogen atom. 10

2.2 The p_z orbitals forming π-bonds lie orthogonal to a nodal plane in which σ bonding occurs. 11

2.3 The graphs $E_{\pm}(k_x)$ for the first Brillouin zone of Benzene. 17

3.1 Segment of Oligophenyl with armchair-edge structure. The repeating unit-cell is bounded by the dashed lines. Note that in all figures, dimensions are scaled to units of the carbon-carbon bond-length, a, where $a = 1.24$ Å. 19

3.2 The wavefunction coefficients are depicted for the six eigenstates, illustrating the bonding and antibonding occurring in particular energy configurations at $k_x = 0$ for single-cell phenyl. Positive coefficients are shown in white and negative coefficients are in black. The states are in order of increasing energy beginning with the ground state (a) and ending with the most energetic state (f). States (b) and (e) are characterized as edge states. 23

3.3 a) Energy bands for single-cell phenyl; b) Energy bands for supercell of three phenyls; c) DOS for both cases remains the same. 26

3.4 An atom of the middle phenyl has its on-site energy changed. 27

3.5 Oligophenyl supercell: a) energy bands no perturbation; b) DOS with no perturbation; c) energy bands with 2.0 eV perturbation; d) DOS with 2.0 eV perturbation. 28

3.6 The band structure (left) and DOS (right) for the oligophenyl with an edge-atom perturbation of 4.0 eV. A three-phenyl supercell has been used. 29

3.7 The DOS for a three-phenyl ribbon (top) and for a seven-phenyl (bottom). Both DOS have a 4.0 eV on-site edge perturbation. The DOS plots differ as expected in the number of dips caused by the joining of the folded bands at the edges of the Brillioun zone. The number of dips corresponds with the number of times the energy bands are folded—three times in the case of former supercell, and seven in the case of the latter. Additional dips occur at $k_x = 0$ which is also an expected result of a repeating potential. 30

3.8 The LDOS at -13.0 eV illustrates the edge-state correspondence with the flat energy-bands for the unperturbed case (top) and the edge-perturbed case (bottom). 31

3.9 The DOS (top) and the LDOS at -13.0 eV (bottom) for a perturbation located along the bond axis. Note that a five-phenyl supercell has been used here. 33

4.1 Segment of Oligoacene with zigzag edge-structure 35

4.2 The repeating unit-cell for the acene system. 35

4.3 a) The band structure for oligoacene. b) DOS for the unperturbed acene system. The unit cell used consists of four carbon atoms. Note $E_F \approx -9.0$ eV. 37

4.4 Edge states of the unperturbed oligoacene at -9.0 eV at the positive X-point. 39

4.5 The locations for each perturbation. Note that the two cases are studied separately. 39

4.6 a) DOS for unperturbed acene ribbon. b) Energy bands for unperturbed acene ribbon. c) Energy bands for acene ribbon with perturbation nearest the bond axis. d) DOS for acene ribbon with perturbation nearest the bond axis. A three-acene supercell is used and the perturbation is 2.0 eV. 40

4.7 DOS for three-acene supercell (bottom) and seven-acene supercell (top). The perturbation is 2.0 eV. 42

4.8 a) LDOS at -9.0 eV for the perturbation nearest the bond axis; b) DOS for perturbation nearest bond axis. 43

4.9 a) LDOS at -9.0 eV for the perturbation on the edge; b) DOS for the edge perturbation. 44

4.10 a) LDOS at -8.5 eV for a 2.0 eV edge perturbation; b) DOS for the edge perturbation. 46

List of Tables

2.1 Energy eigenvalues for benzene (neglecting the hydrogen) 13

2.2 The energy eigenvalues for benzene using periodic boundary-conditions. 18

Acknowledgments

I have been privileged in my life for the many dedicated and devoted teachers who have taken interest in me and from whom I have learned a great deal more than could ever be taught in a single classroom. My thesis advisors here, Tony Cancio and Mahfuza Khatun have been no exception. Their sincere kindness and generosity will forever be remembered by this student, and without which, this project would not have come to fruition. Tony's gracious (and persistant) efforts, in particular, have left me more prepared, more excited, and a bit more confused about physics than would have been possible before. I am wholly grateful.

It was Thom Robertson, our department chair, who kindly supported my travel to the 2008 March Meeting of the American Physical Society in New Orleans, LA and to Argonne National Laboratory in Illinois where I presented this work. Much Thanks! I also owe a debt of gratitude to Bob Cox whose spectacular computer skills saved my life on several occasions. Ron Cosby taught me much of what I know about the formalism of solid state physics—-enjoyably so, at the earliest of hours. I also happily acknowledge the friendly, good advice of Jerry Thomas. My discussions with him—while not directly related to this work—have caused me to recognize that life and wit and perpetual inquiry are as important as the knowledge we gain from them.

To you all, and to those I have terribly forgot to mention, I happily extend a long-overdue, Thank You!

Chapter 1

Introduction

1.1 Nanoscience

The ability of experimenters to grow and synthesize molecular constructions with dimensions on the order of 10^{-9} meters has lead to a field of physics and engineering known as nanoscience or nanotechnology. Within recent decades this area of research has become one of the fastest-growing fields of research world-wide. Nanoscience involves the application of quantum mechanics to individual atoms and molecules in both the atomistic and mesoscopic regimes. This allows one to manipulate matter in a novel way—literally, atom by atom in some cases—while completely understanding the physics of the system.

As a result of this control over matter at such small distance-scales, nanoscience holds the possibility for cutting-edge advances in our ability to ameliorate society. In particular, it has allowed for the construction of new, electronic devices with unusually novel properties upon which our society is increasingly dependent.

An additional consideration for the study of nanoscience, aside from its applications, is the way in which it elucidates the nature of essentially one or two-dimensional

systems. That is, nanotubes and nanoribbons provide a way of understanding the physics of reduced dimensionality without the need for much idealization [2].

1.2 Motivation for the Study

1.2.1 Introduction

Recent experimental advances with graphene sheets and structures continue the possibility of nanoelectronics, where entire circuits could be formed from a sheet of graphene. Allotropes of carbon such as carbon nanotubes (CNTs), buckyballs, nanobrushes, and most recently graphene nanoribbons and strips have been produced experimentally—all with the important property that they exhibit both semiconducting and metallic, electronic behaviors. This makes them prime targets for the development of nano-electrical devices.

Graphene is a single, atomic layer of graphite consisting of a two-dimensional honeycomb structure of sp^2 σ-bonded carbon atoms. Its band structure is unusual because it is metallic in some directions in momentum space and semiconducting in the others. Recent excitement about graphene has come about due to the first, successfull experiments to isolate free-standing two-dimensional graphene sheets [3, 4]. Also, because interconnection and assembly of CNTs have been known to present challenges, the use of graphene has a material substitute in nanoscale devices has become of interest. Moreover, it is believed that the unique electronic properties of CNTs could be obtained if graphene sheets were limited to nanometer-scale dimensions. In fact, new experiments have shown that graphene behaves as either a semiconductor or metal, which has long been the seized-upon property of CNTs [4].

1.2.2 Carbon Nanotubes

The discovery of carbon nanotubes by Iijima in the 1990s [5] has given rise to intensive research on quasi-one-dimensional structures. CNTs are nanometer-diameter cylinders consisting of a single graphene sheet which is wrapped in the form of a tube as illustrated in Figure 1.1. CNTs are grown by combining a source of carbon with a

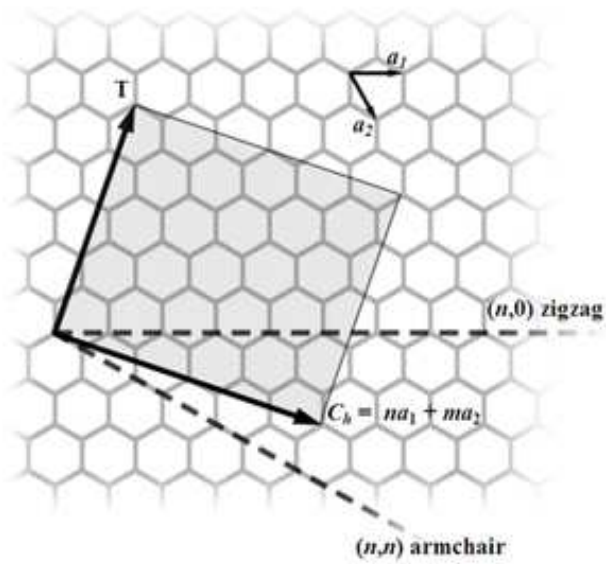

Figure 1.1: The manner in which a graphene sheet is wrapped is represented by a pair of integer-indices, (n, m), which denote a chiral vector, $\vec{C}$, or chirality of the structure. If $m = 0$, the configuration is "zigzag." If $n = m$, the configuration is "armchair." For all other cases, it is simply chiral. The vector, $\vec{T}$, runs along the length of the tube. The tube is folded in such a way that connecting the point described by $\vec{C}$ to its origin constructs a seamless cylinder.

catalytic nanostructured-material such as iron or cobalt at high temperatures. The actual details of the growth process are not well understood [6]. As one of the most promising building blocks for the future development of functional nanostructures, CNTs can be used as one-dimensional quantum wires, optical switches, nanotransistors, and other important electrical components. The individual single-walled CNTs have been predicted to be metallic or semiconducting based upon their diameters and

chiralities [7].

1.2.3 Nanoribbons and Nanostrips

Graphene nanoribbons (GNRs), for which the width of the sheet is confined to be finite while the length is considered infinitely long, have attracted much attention for their unique electronic properties. These include either metallic or semiconducting behavior as a function of ribbon width. This is a result from the experimental achievements with graphene. The ribbons can be grown from mechanical cleavage techniques and also from the sublimation of non-carbon elements from carbon compounds such as SiC [3, 4].

Nanoribbons show distinct electronic properties when compared to two-dimensional graphene, and like CNTs can be classified as either armchair or zigzag GNRs [8] as seen in Figure 1.2. The geometry of the extreme chiralities, armchair and zigzag, are

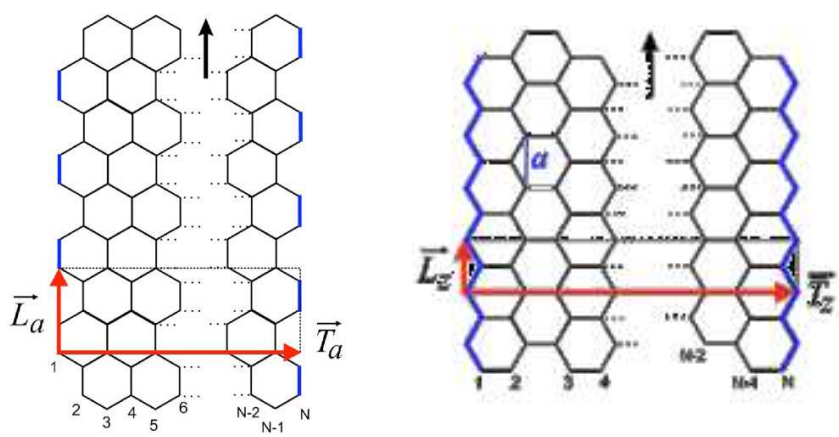

Figure 1.2: Armchair (left) and zigzag nanoribbons (right) [1]. The vector $\vec{L}$ runs along the length of the ribbon, while vector $\vec{T}$ defines the ribbon's width.

realizable in graphene nanoribbons because their edges exhibit these patterns.

Furthermore, it is believed that high-aspect-ratio GNRs with widths between 5 and 10 nm may provide important components in carbon-based quantum electronics because they have structures suitable for in-plane device processing [9, 10].

Recent theoretical analyses of these nanoribbons and chains have focused on the effect of disorder on the electronic structure. Furthermore, any such finite strips made by experimenters are likely to have irregular edges, that is, an edge-disorder [8]. The exact nature of this disorder affects the strips properties as well as provides a means of tailoring those properties to particular applications. Also, an actual strip of finite size has the ability to be bonded by a species of atoms not of the composition of the rest of the strip—that is, impurity atoms could be introduced at the edges where the strips are truncated. It has been found for example that in the case of graphene nanostrips, hydrogen-terminated zigzag-edges are better initial targets for ballistic-transport device-applications, while the sensitivity of hydrogen-terminated armchair-edge strips with edge disorder might make them useful as sensors. The width of the strips also affects the strips' properties, such as the conductance. Additionally, and more recently as compared to CNTs, it is considered to be highly probable that nanostrips will experience a higher degree of interaction with the substrate upon which they are grown. The substrate interaction is of importance because experimentally grown structures, e.g. CNTs and nanostrips, naturally incur disorder and this can limit the potential performance of devices made from them [10].

1.3 Tight-Binding Overview

The tight-binding method has long been a standard approach for electronic structure calculations since it was first developed by Bloch in 1928 [11]. Because it makes use

of symmetries and semi-empirical parameters as opposed to explicit functions and exact forms, it often provides a first step in understanding the electronic behavior of a physical system.

Central to the tight-binding approach is the concept of localized orbitals: The wavefunction is linearly decomposed into a basis of highly-localized atomic-states. The Hamiltonian matrix is then readily constructed and diagonalized.

Employed in this work, however, is a semi-empirical approach developed by Walter A. Harrison [12] where the explicit form of the atomic basis-functions is not used. Instead, parameters which become the values of the matrix elements of the Hamiltonian, are calculated from a standardized formula, which has been well-investigated.

1.4 The Thesis Work

This thesis explores the electronic structure of oligophenyl and oligoacene. Both are examples of extreme, one-dimensional, graphene nanoribbons. Here we model each as an infinite system. More specifically, the oligophenyl and oligoacene are chains of benzene, bonded together in the armchair and zigzag directions, respectively, and thus relate well to the work being done on other types of graphene nanostrips and sheets. The electronic structure and density of states is determined using a simple tight-binding method. The local density of states is also discussed. Also presented in this work is the effect of perturbations to the on-site energy of one of the carbon atoms within a repeating supercell.

1.5 Preview

A brief preview of this work is now offered with an explaination of how each proceeding chapter addresses the research done in a topical fashion. The next chapter, Chapter 2, will describe the formalism of the tight-binding technique which is used exclusively in all energy calculations. In the context of that discussion the tight-binding formalism will be applied to two systems: the single benzene-ring without its hydrogen atoms, then benzene with hydrogen using periodic boundary-conditions for which analytical solutions are readily obtained. Therefore, much of Chapter 2 has been devoted to the mathematical formalism that is used in the subsequent calculations of the oligophenyl and oligoacene systems.

Chapter 3 presents the description and analysis of the oligophenyl. This includes the energy-band structure and the density of states for the perturbed and unperturbed systems. The relative wavefunction-coefficients and the local density of states are plotted and shown pictorially.

Chapter 4 presents a similar analysis for the oligoacene system.

Chapter 5 is a conclusion which discusses the final results of this collective work and prognosticates on new avenues to be taken.

The appendices contain samples of the python coding used in the calculations for the results of Chapters 3 and 4.

Chapter 2

The Tight-Binding Model

2.1 Synopsis

As discussed in Chapter 1, the tight-binding model is the technique often employed by researchers to obtain a quick and often approximate result for the electronic structure of many systems. This model is most widely used by scientists in physics, chemistry and material science. Tight-binding methods are especially popular because of their efficiency in large simulations [11]. The term tight-binding is derived from the basis of atomic orbitals into which the electron wavefunction is decomposed.

The procedure itself is relatively straight-forward. The wavefunction is written as a linear expansion of a complete set of atomic basis functions, or orbitals. Each term in the expansion corresponds to a state of fixed energy and is independent of the other terms [11]. The acronym LCAO—or linear combination of atomic orbitals is used to refer to such a formulation and is often synonymous with the term, tight-binding.

Mentioned in the introduction is the fact that the tight-binding approach assumes an appropriate form of the Hamiltonian in terms of overlap matrix-elements and on-site matrix-elements. The overlap elements describe the strength of the nearest-

neighbor interactions—the only interactions an electron of one atom experiences, save the electric potential it experiences from the atom to which it is bound. The latter is referred to as the on-site energy. This is done without need of direct access to the explicit form of the orbital functions. Only their symmetry, i.e. whether they are describing s or p states is needed. The values of the orbital overlaps are usually obtained from experiment or by fitting a theoretical formula to experiment, the latter being the method of Walter Harrison and consequently what will be used in this work [12].

2.2 Benzene (Neglecting the Hydrogen)

I will now present the tight-binding model by applying its formalism to a toy example of the single benzene molecule. As shown in Figure 2.1 benzene consists of six carbon atoms bonded together in the hexagonal pattern with hydrogen atoms attached to each carbon. The electron configuration of carbon in this molecule is: $1s^2 2s^1 2p_x^1 2p_y^1 2p_z^1$. It is reasonable to consider only the p_z electrons forming π-bonds which are orthogonal to the plane of the hexagon. The electrons comprising the configuration, $2s^1 2p_x^1 2p_y^1$, have orbitals lying in the hexagonal plane and are involved in σ-bonding resulting from the sp^2-hybridization. They form strong C-C bonds and decouple from the π-conduction bands. Because the σ-bands associated with these electrons lie far from the Fermi energy, E_F, and are thus not involved in transport, I will only concern this calculation with the p_z-electrons [10]. The hydrogen atoms are involved in the σ-bonding. The subsequent calculations for the oligophenyl and oligoacene systems will also follow this approach. Also for this example, I will omit the hydrogen atoms from the explicit calculation, i.e. their orbitals will not be included in the expansion of the electron's wavefunction. I will however develop the mathe-

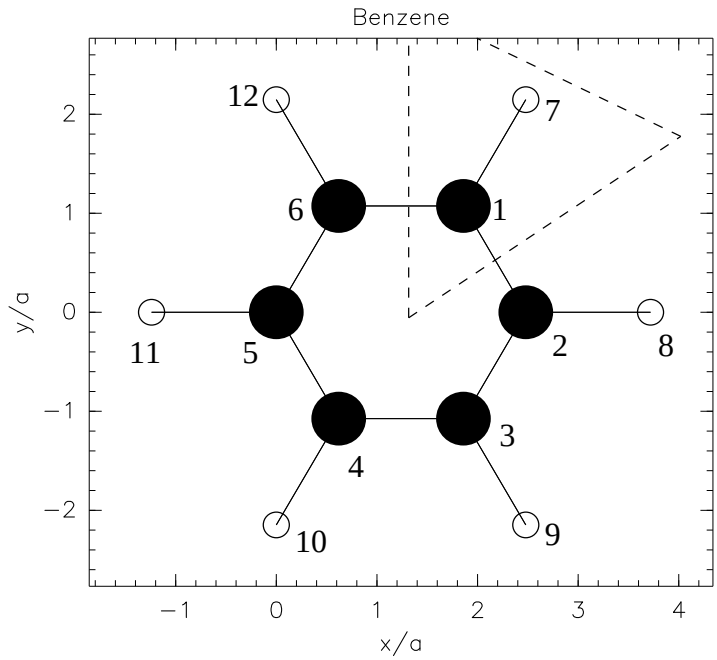

Figure 2.1: The benzene molecule has six carbon atoms (black) bonded together in the hexagonal shape with an outer ring of hydrogen atoms (white) bonded to each carbon. The repeating unit-cell (used in Section 2.3) is highlighted by the dashed lines and consists of one carbon atom and one hydrogen atom.

matical formalism of the tight-binding method analytically by adding the hydrogen atoms into the calculation in the proceeding section.

The benzene molecule then, with this electronic consideration, reduces to six carbon atoms each of which contributes one electron to form π-bonds orthogonal to the nodal plane. Figure 2.2 illustrates this situation. Using the method developed

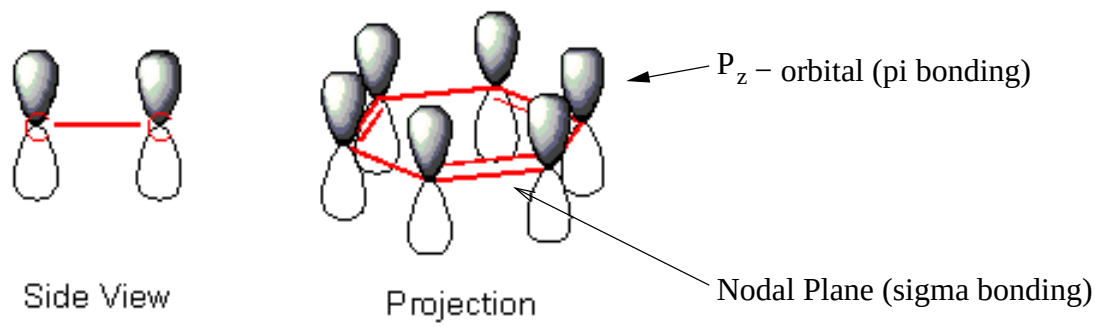

Figure 2.2: The p_z orbitals forming π-bonds lie orthogonal to a nodal plane in which σ bonding occurs.

by W. A. Harrison we construct a tight-binding Hamiltonian, $\hat{H}$, to operate on the wavefunction by

$$\hat{H}\psi_n = E_n\psi_n. \tag{2.1}$$

The Hamiltonian operator has the form, $\hat{H} = \frac{-\hbar^2}{2m}\vec{\nabla}^2 + V(\vec{r})$, where $V(\vec{r})$ is the potential-energy function of the electron. The wavefunction, $|\psi\rangle$, can be written as a linear combination of atomic orbitals—in this case the p_z-orbitals—centered on each atom such that

$$|\psi\rangle = \sum_i c_i|\varphi_i\rangle, \tag{2.2}$$

as is done by Harrison [12]. The matrix elements of the Hamiltonian then take the form, $H_{ij} = \langle\varphi_i|H|\varphi_j\rangle$. According to the tight-binding model the carbon on-site energy, $\epsilon_p = \langle\varphi_i|H|\varphi_i\rangle$. The remaining matrix-elements of the Hamiltonian, $\langle\varphi_i|H|\varphi_j\rangle$, are either identically zero or equal to an overlap parameter, V_{ijk}. V_{ijk} goes

as the inverse of the square of the internuclear distance such that

$$V_{ijk} = \eta_{ijk}\frac{\hbar^2}{md^2}, \tag{2.3}$$

where d is the internuclear distance (in this case 1.24 Å), m is the electron mass, and the values for η_{ijk} are four universal constants related to the orbital shape (i, j) and type of bond (k), such as $ss\sigma$ or $pp\pi$ [12]. Therefore the overlap elements, $V_{ijk} = \langle\varphi_i|H|\varphi_j\rangle$, for $i \neq j$ and when i and j correspond to nearest-neighbors only. When i and j are not nearest-neighbors, $V_{ijk} = \langle\varphi_i|H|\varphi_j\rangle = 0$.

Because only the p_z-electrons of hydrogen and carbon which form π-bonds are of concern here, the matrix elements described above are properly evaluated above to be $V_{pp\pi} = -4.01$eV. It is interesting to note that the value of the overlap parameter, in particular the value of η_{ijk}, is independent of the species of the atoms involved; only the orbital type and bond affect the result. The on-site energy, $\epsilon_p = -8.97$eV, is also obtained from tabulated values [12].

When the Hamiltonian is cast as a matrix, $\mathbf{H}$, it has the form,

$$\mathbf{H} = \begin{pmatrix} \epsilon_p & V_{pp\pi} & 0 & 0 & 0 & V_{pp\pi} \\ V_{pp\pi} & \epsilon_p & V_{pp\pi} & 0 & 0 & 0 \\ 0 & V_{pp\pi} & \epsilon_p & V_{pp\pi} & 0 & 0 \\ 0 & 0 & V_{pp\pi} & \epsilon_p & V_{pp\pi} & 0 \\ 0 & 0 & 0 & V_{pp\pi} & \epsilon_p & V_{pp\pi} \\ V_{pp\pi} & 0 & 0 & 0 & V_{pp\pi} & \epsilon_p \end{pmatrix}. \tag{2.4}$$

Based upon the discussion described earlier, it is easy to see that each element in the Hamiltonian delineates an interaction. Element, $H_{14} = H_{41} = 0$, e.g, represents the fact that when numbering the carbon atoms from one to six, atom one and four

Energy (eV)
-17.00
-12.98
-12.98
-5.00
-5.00
-0.94

Table 2.1: Energy eigenvalues for benzene (neglecting the hydrogen)

do not interact because they are not nearest-neighbors. Likewise, atoms one and six have an overlap interaction and thus, $H_{16} = H_{61} = V_{pp\pi}$.

The Hamiltonian is Hermitian and symmetric about the diagonal. Upon diagonalizing the matrix, the six energy eigenvalues are obtained and given in Table 2.1. From these values and the fact that two electrons can occupy each state, the last filled-state has an energy of -12.98 eV and the first unoccupied-state has an energy of -5.00 eV. Thus, the HOMO-LUMO gap for benzene is 7.98 eV. In the next section the addition of the hydrogen atom will prove to negligibly affect this band gap.

2.3 Tight-binding Formalism and Benzene

To develop the mathematical detail of the tight-binding model, I return to the example of the benzene molecule. This approach will introduce the very important concept of periodic boundary-conditions for systems such as this. Unfortunately, in an analysis where we wish to use a two-atom basis of carbon and hydrogen for benzene and still apply the p_z-electron calculation, the result is not realistic for low-energy states. It would require the hydrogen electrons to occupy a p_z-orbital which constitutes an excited state of the molecule. In the subsequent calculations and the results of this thesis work, only the lowest energy-state will be of interest. Nevertheless, I believe this toy example has great utility in demonstrating the basic concepts of the tight-binding

model.

To begin, the repeating unit-cell of the benzene molecule as shown in Figure 2.1 is identified as containing one carbon atom and one hydrogen atom. Note that there are $N = 6$ cells in the system. Identifying a repeating cell, as in this case, is important because it allows for the electronic structure of the system to be determined by studying only a single unit cell, I, with the caveat that we include the fact that each cell is connected to its neighboring cells.

I will assume that the wavefunction can be expressed in terms of the Bloch function and written as

$$\psi(\vec{r}) = e^{i\vec{k}\cdot\vec{r}}u(\vec{r}), \tag{2.5}$$

where $\vec{r}$ is the location of the electron anywhere in the repeating structure and $u(\vec{r})$ is a periodic function with the periodicity of the structure. Upon making the tight-binding imposition we decompose ψ into a LCAO, so that

$$|\psi\rangle = \sum_{I=1}^{N} e^{i\vec{k}\cdot\vec{R}_I}(\ c_1|\alpha_I\rangle + c_2|\beta_I\rangle\ ) \tag{2.6}$$

where the coefficients, c_1 and c_2, are the same for all I, and $|\alpha_I\rangle$ and $|\beta_I\rangle$ are the carbon and hydrogen atomic-orbitals on cell I, respectively. $\vec{R}_I$ is a vector from the origin to cell I. Also note that I have switched to bra-ket notation and hence, $|\psi\rangle$, $|\alpha_I\rangle$, and $|\beta_I\rangle$, are functions of $\vec{r}$. Writing the expression for $|\psi\rangle$ more compactly

$$|\psi\rangle = \sum_{I=1}^{N}[|\alpha_I\rangle\langle\alpha_I|\psi\rangle + |\beta_I\rangle\langle\beta_I|\psi\rangle] \tag{2.7}$$

and applying the Hamiltonian operator, $\hat{H} = \frac{-\hbar^2}{2m}\vec{\nabla}^2 + V(\vec{r})$, where $V(\vec{r})$ is the

potential-energy function of the electron, we have

$$\sum_{J}^{N} \hat{H}[|\alpha_J\rangle\langle\alpha_J|\psi\rangle + |\beta_J\rangle\langle\beta_J|\psi\rangle] = E\sum_{J}^{N}[|\alpha_J\rangle\langle\alpha_J|\psi\rangle + |\beta_J\rangle\langle\beta_J|\psi\rangle]. \tag{2.8}$$

Multiplying both sides of Equation 2.8 by $\langle\alpha_I|$ gives,

$$\langle\alpha_I|\sum_{J}^{N} \hat{H}[|\alpha_J\rangle\langle\alpha_J|\psi\rangle + |\beta_J\rangle\langle\beta_J|\psi\rangle] = \langle\alpha_I|E\sum_{J}^{N}[|\alpha_J\rangle\langle\alpha_J|\psi\rangle + |\beta_J\rangle\langle\beta_J|\psi\rangle] \tag{2.9}$$

$$\begin{aligned}
&= \langle\alpha_I|H|\alpha_I\rangle\langle\alpha_I|\psi\rangle \\
&+\langle\alpha_I|H|\alpha_{I+1}\rangle\langle\alpha_{I+1}|\psi\rangle + \langle\alpha_I|H|\alpha_{I-1}\rangle\langle\alpha_{I-1}|\psi\rangle \\
&+\langle\alpha_I|H|\beta_I\rangle\langle\beta_I|\psi\rangle + \langle\alpha_I|H|\beta_{I+1}\rangle\langle\beta_{I+1}|\psi\rangle \\
&+\langle\alpha_I|H|\beta_{I-1}\rangle\langle\beta_{I-1}|\psi\rangle = E[[\langle\alpha_I|\alpha_I\rangle\langle\alpha_I|\psi\rangle \\
&+\langle\alpha_I|\beta_I\rangle\langle\beta_I|\psi\rangle] + [\langle\alpha_I|\alpha_{I+1}\rangle\langle\alpha_{I+1}|\psi\rangle \\
&+\langle\alpha_I|\beta_{I+1}\rangle\langle\beta_{I+1}|\psi\rangle] + [\langle\alpha_I|\alpha_{I-1}\rangle\langle\alpha_{I-1}|\psi\rangle \\
&+\langle\alpha_I|\beta_{I-1}\rangle\langle\beta_{I-1}|\psi\rangle]].
\end{aligned}$$

After multiplying by the ket, the sum over J returns non-zero inner-products for only the terms where $J = I, I+1, I-1$ because of the nearest-neighbor consideration. This condition also forces non-nearest-neighbor overlap-terms in the lines following Equation 2.9 to vanish, e.g., the term $\langle\alpha_I|H|\beta_{I+1}\rangle\langle\beta_{I+1}|\psi\rangle$ must vanish. Also, the inner products of the form $\langle\alpha_m|\alpha_n\rangle$ and $\langle\alpha_m|\beta_n\rangle$ are such that $\langle\alpha_m|\alpha_n\rangle = \delta_{nm}$ and $\langle\alpha_m|\beta_n\rangle = 0$. This is due to the tight-binding consideration that atomic orbitals on different atoms have negligible overlaps.

To cast the remaining inner-products in a matrix form, they must be evaluated according to the tight-binding model. Similarly, the on-site energy, ϵ_p, results from

evaluating the remaining inner-products of the form, $\langle \alpha_I | H | \alpha_I \rangle$. From tabulated values it is found that the on-site energy for hydrogen, ϵ_p^h, is -3.4 eV, and the on-site energy for carbon, ϵ_p^c, is -8.97 eV [12]. Upon substituting these parameters and simplifying, Equation 2.9 reduces to,

$$\epsilon_p^c e^{ik_x Ia} c_1 + V_{pp\pi} e^{ik_x (I+1)a} c_1 + V_{pp\pi} e^{ik_x (I-1)a} c_1 + V_{pp\pi} e^{ik_x Ia} c_2 = E\ c_1 e^{ik_x a}. \tag{2.10}$$

Here a is the bond length between nearest-neighbor atoms.

Similarly, multiplying Equation 2.8 by $\langle \beta_I |$ yields the corresponding equation,

$$\epsilon_p^h e^{ik_x Ia} c_2 + V_{pp\pi} e^{ik_x Ia} c_1 = E\ c_2 e^{ik_x a}. \tag{2.11}$$

Dividing each term in both Equation 2.10 and 2.11 by $e^{ik_x a}$ gives the matrix equation,

$$\begin{pmatrix} \epsilon_p^c + 2V_{pp\pi} cos(k_x a) & V_{pp\pi} \\ V_{pp\pi} & \epsilon_p^h \end{pmatrix} \begin{pmatrix} c_1 \\ c_2 \end{pmatrix} = E_n(k_x) \begin{pmatrix} c_1 \\ c_2 \end{pmatrix}. \tag{2.12}$$

The energy, E, has now become a function of the magnitude of the wavevector k_x, which has units of 2/7.62 Å in all calculations and plots. This is now referred to as the dispersion relation, $E(k_x)$. Together with the rank of the matrix fixing the number of n eigenvalues, each of which is a function of k_x, the numbers, k_x and n, determine the quantization of the system. The 2 x 2 Hamiltonian, **H**, of Equation 2.12

is easily diagonalized to return the energy eigenvalues with the requirement det(**H**-**I**E)=0. From Equation 2.12 and the imposition that det(**H**-**I**E)=0, the resulting energy bands for benzene are given by,

$$E_{\pm} = \frac{\epsilon_p^c + \epsilon_p^h + 2V_{pp\pi}cos(k_x a)}{2} \pm \frac{\sqrt{[\epsilon_p^c + \epsilon_p^h + 2V_{pp\pi}cos(k_x a)]^2 - 4[2\epsilon_p^c V_{pp\pi}cos(k_x a) + \epsilon_p^c \epsilon_p^h - V_{pp\pi}^2]}}{2}. \quad (2.13)$$

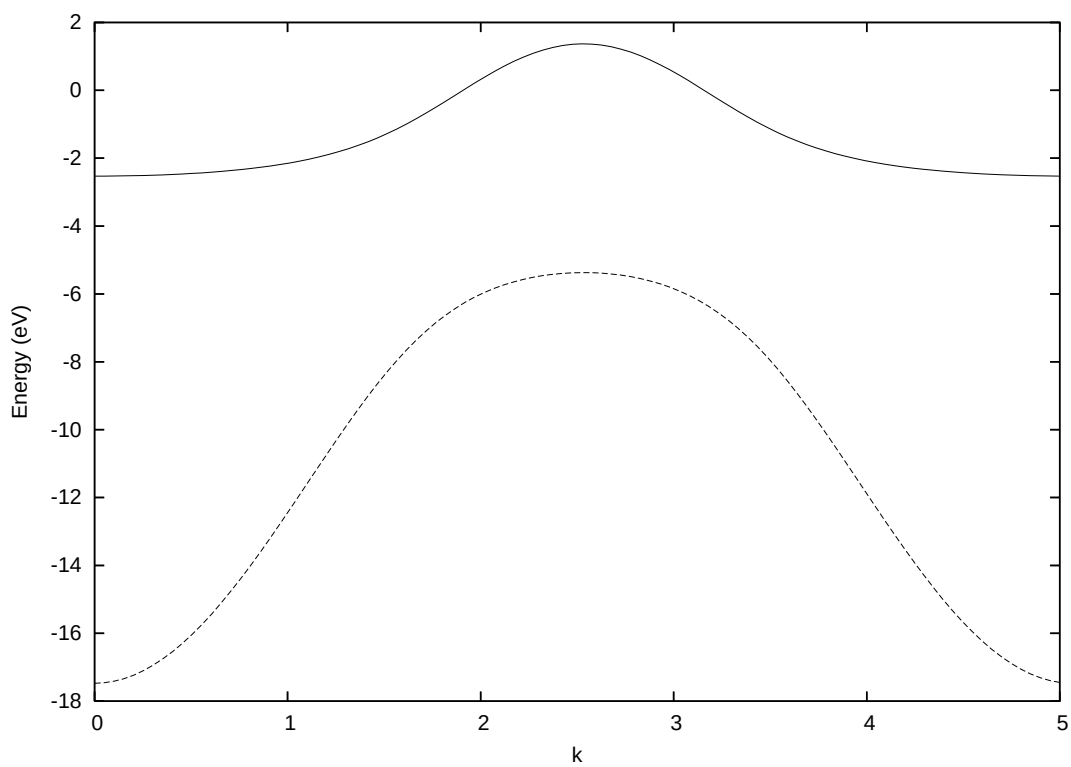

Figure 2.3: The graphs $E_{\pm}(k_x)$ for the first Brillouin zone of Benzene.

When $E_{\pm}$ is plotted in Figure 2.3, it shows two continuous energy-bands. This is misleading. In fact, only certain, discrete values of k_x are allowed: 0, $1/a$, $2/a$, $3/a$, $4/a$, and $5/a$ as indicated in Table 2.2. This restriction is a consequence of the periodicity of the discrete system. Here we have a single, benzene molecule modeled

k_x	**Eigenvalue (eV)** E_-	**Eigenvalue (eV)** E_+
0	-17.69	-2.7
0.81	-13.93	-2.46
1.61	-7.42	-0.93
2.42	-5.55	1.21
3.23	-7.42	-0.93
4.03	-13.93	-2.46

Table 2.2: The energy eigenvalues for benzene using periodic boundary-conditions.

by six repeating-cells, each of which consists of two atoms. Therefore it is appropriate to approximate the system as a ring of unit-cells where each unit-cell is separated by distance, s. In that case, $\psi \sim e^{ik_x s} = e^{ik_x a\theta}$, where θ is an azimuthal angle on the circle. Enforcing the periodic condition that, $e^{ik_x a\ 2\pi} = e^{ik_x a\ 0} = 1$, yields

$$k_x a 2\pi = 2\pi n, \tag{2.14}$$

$$k_x = n/a, \tag{2.15}$$

where n is an integer and θ is determined from the geometry of the benzene structure to be $\pi/3$.

The ground-state energy of this system is found to be -17.7 eV and the HOMO-LUMO gap is 6.5 eV, with the HOMO and LUMO states occurring at $k_x = 3/a$. The accuracy of the tight-binding model for benzene is relatively good considering that B3LYP and BLYP Density Functional Theory yield a range of 5.772 - 7.658 eV using the basis set STO-3G for the HOMO-LUMO gap [13].

Chapter 3

Oligophenyl

3.1 Unperturbed Oligophenyl

3.1.1 Introduction

Using the same procedure described in Chapter 2, I will now apply the tight-binding model to an infinitely repeating chain of benzene molecules whose hydrogen atoms have been omitted. This chain of carbon hexagons—or phenyls—is referred to as oligophenyl and depicted in Figure 3.1

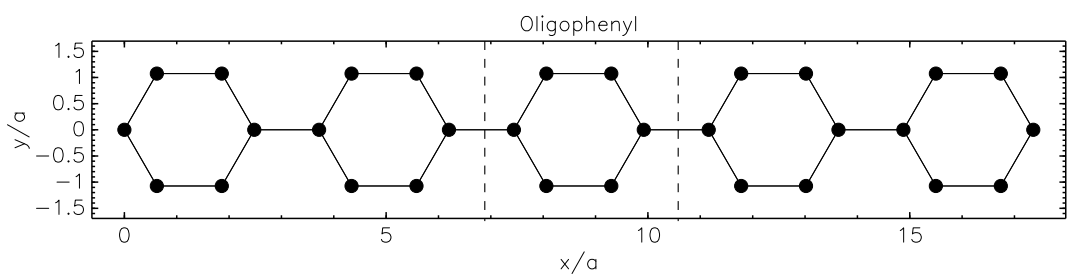

Figure 3.1: Segment of Oligophenyl with armchair-edge structure. The repeating unit-cell is bounded by the dashed lines. Note that in all figures, dimensions are scaled to units of the carbon-carbon bond-length, a, where $a = 1.24$ Å.

It is reasonable to consider only the p_z-electrons forming π-bonds which are or-

thogonal to the plane of the hexagon. As mentioned in Chapter 2, the electrons comprising the configuration, $2s^1 2p_x^1 2p_y^1$, have orbitals lying in the hexagonal plane and are involved in σ-bonding. They form strong C-C bonds and decouple from the π-conduction bands. Also, because the σ-bands associated with these electrons lie far from the Fermi energy, E_F, and are thus not involved in transport properties, I again will only concern this calculation with the p_z-electrons [10].

3.1.2 Energy and Density of States

To begin the electronic-structure calculation it is necessary to identify the repeating unit-cell from which the entire system can be constructed. Note that the same notation used in Chapter 2 will be adopted here. In this case it is easily seen that the repeating cell consists of a single, carbon hexagon of lattice constant, $A = 3a$. Applying the same prescription as described in Chapter 2, the wavefunction is decomposed into a set of linearly-independent basis-functions (atomic orbitals) and the operator, $\hat{H}$, is applied. Upon considering only nearest-neighbor terms Equation 2.1 can be written in matrix form where the Hamiltonian, $\mathbf{H}$ is given by,

$$\mathbf{H} = \begin{pmatrix} \epsilon_p^c & Ve^{ik_x a/2} & 0 & 0 & 0 & Ve^{-ik_x a} \\ Ve^{-ik_x a/2} & \epsilon_p^c & Ve^{-ik_x a/2} & 0 & Ve^{ik_x a} & 0 \\ 0 & Ve^{ik_x a/2} & \epsilon_p^c & Ve^{-ik_x a} & 0 & 0 \\ 0 & 0 & Ve^{ik_x a} & \epsilon_p^c & Ve^{-ik_x a/2} & 0 \\ 0 & Ve^{-ik_x a} & 0 & Ve^{ik_x a/2} & \epsilon_p^c & Ve^{ik_x a/2} \\ Ve^{ik_x a} & 0 & 0 & 0 & Ve^{-ik_x a/2} & \epsilon_p^c \end{pmatrix}, \quad (3.1)$$

where $V = V_{pp\pi}$.

Diagonalizing the Hamiltonian (see Appendix A) yields the band structure for

the first Brillouin zone shown in Figure 3.3a. There are six energy bands. The three bands near the bottom constitute the valence bands while the top-three, unfilled bands make up the conduction bands. The HOMO-LUMO gap is found to be 3.3 eV and Fermi energy, $E_F = -9.0$ eV. As such, the oligophenyl is semiconducting. Interestingly here, $E_F = \epsilon_p^c$. This situation is similar to the electronic structure of two carbon atoms bonded together, where exactly one state of bonding and one of antibonding is found from the 2 x 2 Hamiltonian.

Also shown is the density of states (DOS) for the system. The DOS is determined computationally (see Appendix A) using the final relation,

$$\text{DOS} = \sum_i \frac{1}{2\pi} \int \delta(E_{ik_x} - E) dk \approx \frac{1}{N} \sum_{i,k_x} e^{-(E_{ik_x}-E)^2/k_B T}, \tag{3.2}$$

where E is some energy in the first Brillouin zone, E_{ik_x} is the energy of band i and wavevector $\vec{k}$, N is the number of points in k-space, and $k_B T$ has been set at 0.2 eV. The DOS describes the number of states per lattice length per unit energy. Here the slight activation of temperature is necessary because the calculation is done computationally and an analytic form of $E(k_x)$ is not found. Therefore, the approximation on the right-hand side of Equation 3.2 is used which includes an adjustable parameter in the form of $k_B T$, while an effort is made to avoid unnecessary thermal-broadening. The code then runs over discrete values of $\vec{k}$ with a set increment. The utility of the temperature parameter thus allows for the sharp, discrete spikes of the delta function to broaden into a recognizable continuum.

At $k_x = 0$, states showing the localization of the electron wavefunction are realizable. The relative coefficients of the wavefunction are shown in Figure 3.2 for each of the six energy values at the Γ-point. The states are shown in order of increasing energy (from a-f) beginning with the ground state (3.2a) where the system is in a

state of total bonding. Anti-bonding is then introduced in each successive state to increase the energy, ending with the most energetic state (3.2f) where each atom forms anti-bonds with its neighbors.

3.1.3 Symmetries and Edge States

The oligophenyl has the structure of an extreme-armchair nanoribbon and possesses certain features not found in carbon nanotubes or in solids. Most noticeable are the symmetries of the wavefunction. As seen in Figure 3.2, even and odd mirror-symmetries are present. The state shown in Figure 3.2f, for instance, is invariant under the mirror exchange of coefficients about the bond axis.

As mentioned in the previous section, the Fermi energy was found to be equal to the carbon on-site-energy. This demonstrates a special, electron-positron symmetry, i.e. an exact exchange between occupied and unoccupied states. This is also detectable from the fact that the filled and unfilled energy-bands are symmetric about the Fermi energy.

Of interest are the two states where the wavefunction is nearly zero except along the edges of the phenyl (see Figure 3.2b,e.) These edge states are unique to systems like nanoribbons. They are not seen in two-dimensional graphene. The special characteristics of the edge state play a large role in determining the density of states near the Fermi level for graphite networks on a nanometer scale. Prior theoretical work has shown however that graphite networks with armchair edges do not exhibit a special, edge state at the Fermi energy [9, 14–17]. The effect of the ribbon's width on these edge states has also been studied and it has been shown that the ribbon's width (y-direction), N, determines whether the system is metallic or insulating. More precisely when $N = 3M - 1$, where M is an integer, the system is metallic. For the

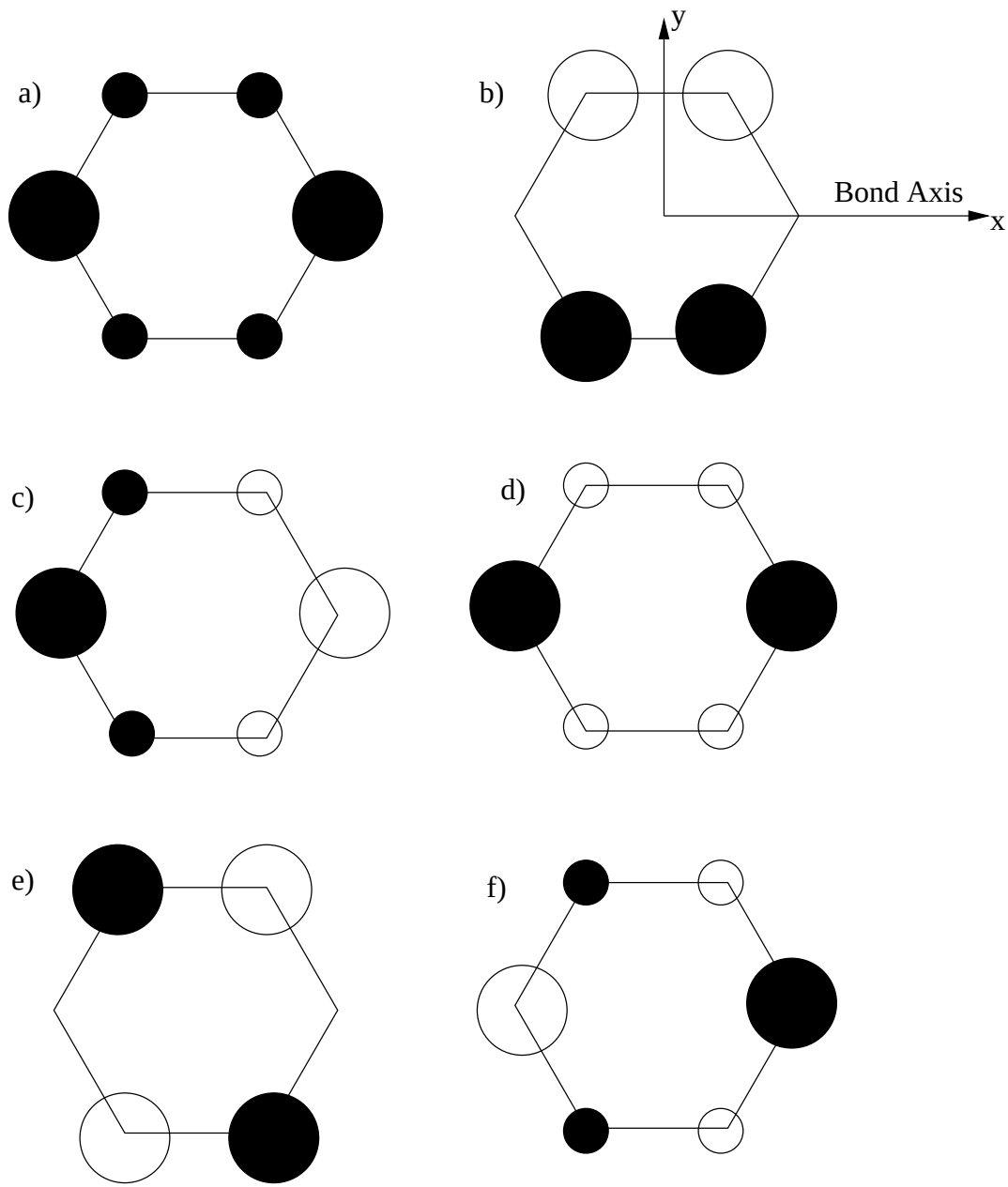

Figure 3.2: The wavefunction coefficients are depicted for the six eigenstates, illustrating the bonding and antibonding occurring in particular energy configurations at $k_x = 0$ for single-cell phenyl. Positive coefficients are shown in white and negative coefficients are in black. The states are in order of increasing energy beginning with the ground state (a) and ending with the most energetic state (f). States (b) and (e) are characterized as edge states.

insulating armchair-ribbons the band gap decreases with increasing ribbon width and approaches zero in the limit of very large N. Moreover, the band structure of two-dimensional graphite is almost reproduced by that of a wide, armchair ribbon [9].

In the extreme case (minimal width and $N = 3$) of the oligophenyl presented here, we do see the appearance of two other, flat bands depicted in Figure 3.2 and our system is semiconducting as expected. Electrons and holes in these states have an infinite mass. Because the oligophenyl is an infinite system, an infinite number of states exist in the flat bands, and a sharp peak in the density of states can be seen here. Further more, the edge states do not permit conductance because nearly all the charge-density is localized on the edges, while the path for conductance is along the center (bond axis).

3.2 Perturbed Oligophenyl

3.2.1 Introduction

It is interesting to examine the effect of disorder in nanoribbons and other nanostructures. Disorder is known to affect the transport properties in nanostrips, favorably or unfavorably altering their ability to be used as ballistic device-applications [10]. Also, because disorder is naturally introduced when these nanostructures are synthesized, it is useful to extract the physics of realistic models.

3.2.2 Perturbing the Oligophenyl

Disorder is introduced by adjusting the value of the on-site-energy matrix-elements for specific atoms in the repeating unit-cell. This mimics well the effects of substrate-induced disorder on finite nanostrips [10], which are very similar to our extreme

system. Because the system is infinite, it is necessary to enlarge the unit cell of Figure 3.1 to a supercell which must include at least three phenyls. Perturbing a single phenyl and using it as the unit cell would over-emphasize periodic effects, making it difficult to discriminate between the interesting features of the disorder and the anticipated effects, e.g. Bragg scattering.

Before we speak of perturbative effects, it is important to point out that the size, itself, of the repeating cell is arbitrary and has no effect on the electronic structure or DOS as long as the system is the same. Figure 3.3 compares the electronic structure of the single-cell case with that of a three-phenyl supercell. Figure 3.4 now shows where the on-site energy of a single carbon atom on the edge of the ribbon is to be slightly perturbed. Diagonalizing the perturbed Hamiltonian (see Appendix B) gives the band structure and the corresponding density of states shown in Figure 3.5 in the reduced-zone scheme. The value of the HOMO-LUMO gap, itself, remains unchanged by the doping while the energy bands broaden, or flatten out for large values of k_x in comparison to the unperturbed case. Most interestingly, the three-fold degeneracy of the flat band which is seen in Figure 3.5a,c (between -14 and -12 eV), is partially lifted by the asymmetry introduced by the on-site energy-change. Increasing the perturbation to 4.0 eV flattens the bands which is shown in Figure 3.6. It is also important to note that when comparing Figure 3.5 and Figure 3.6 one finds that increasing the strength of the perturbation negligibly shrinks the width of the HOMO-LUMO gap. The change is essentially undetectable when comparing the unperturbed case with that of only a 2.0 eV perturbation.

The effects of Bragg scattering due to the periodic nature of the disorder is readily visible through the band gaps at the Brillouin zone edges and at $k_x = 0$. Figure 3.7 compares the DOS for a ribbon with a three-phenyl supercell to that with a seven-phenyl supercell. The interesting effects of the degeneracy-lifting and the

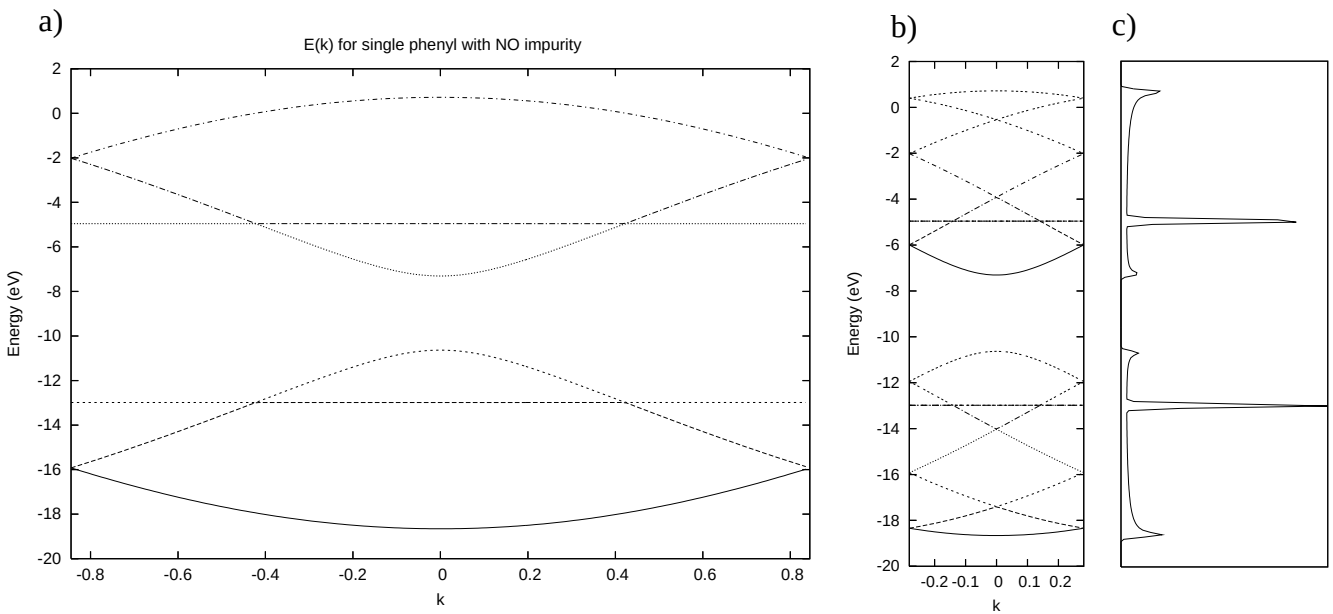

Figure 3.3: a) Energy bands for single-cell phenyl; b) Energy bands for supercell of three phenyls; c) DOS for both cases remains the same.

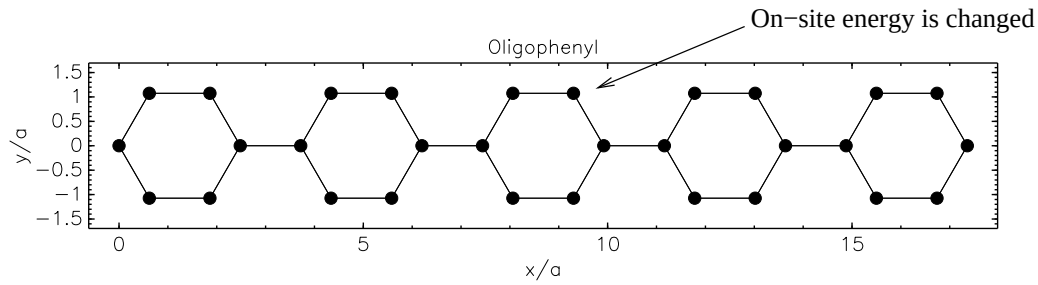

Figure 3.4: An atom of the middle phenyl has its on-site energy changed.

band-broadening, mentioned earlier, are visible in the peaks near those of the two flat bands. These non-periodic effects are distinguishable because their corresponding peaks in the DOS do not differ with the size of the supercell. Conversely, the expected, periodic effects from the band-folding, where corresponding dips in the DOS are apparent, increase in number with the size of the supercell. These effects are not representative of the more interesting effects of the disorder. Also, an analysis of a 2.0 eV perturbation strength as opposed to a higher strength seems to better de-emphasize the effects of the Bragg scattering.

3.2.3 Local Density of States

It is also possible to apply the disorder to an atom of the phenyl which is along the bond axis. To contrast this with the edge impurity, the local density of states (LDOS),

$$\text{LDOS} \sim \sum_i \int C^*_{ik_x} C_{ik_x}\ \delta(E_{ik_x} - E) dk \approx \frac{1}{N} \sum_{i,k_x} C^*_{ik_x} C_{ik_x}\ e^{-(E_{ik_x}-E)^2/k_B T}, \qquad (3.3)$$

is determined by computational means (see Appendix A.) In general, the LDOS modulates the DOS by the localization of the wavefunction at some location, $\vec{r}$, in real space. However, in this work we obtain the *coefficients*, C_{ik_x} of the wavefunction,

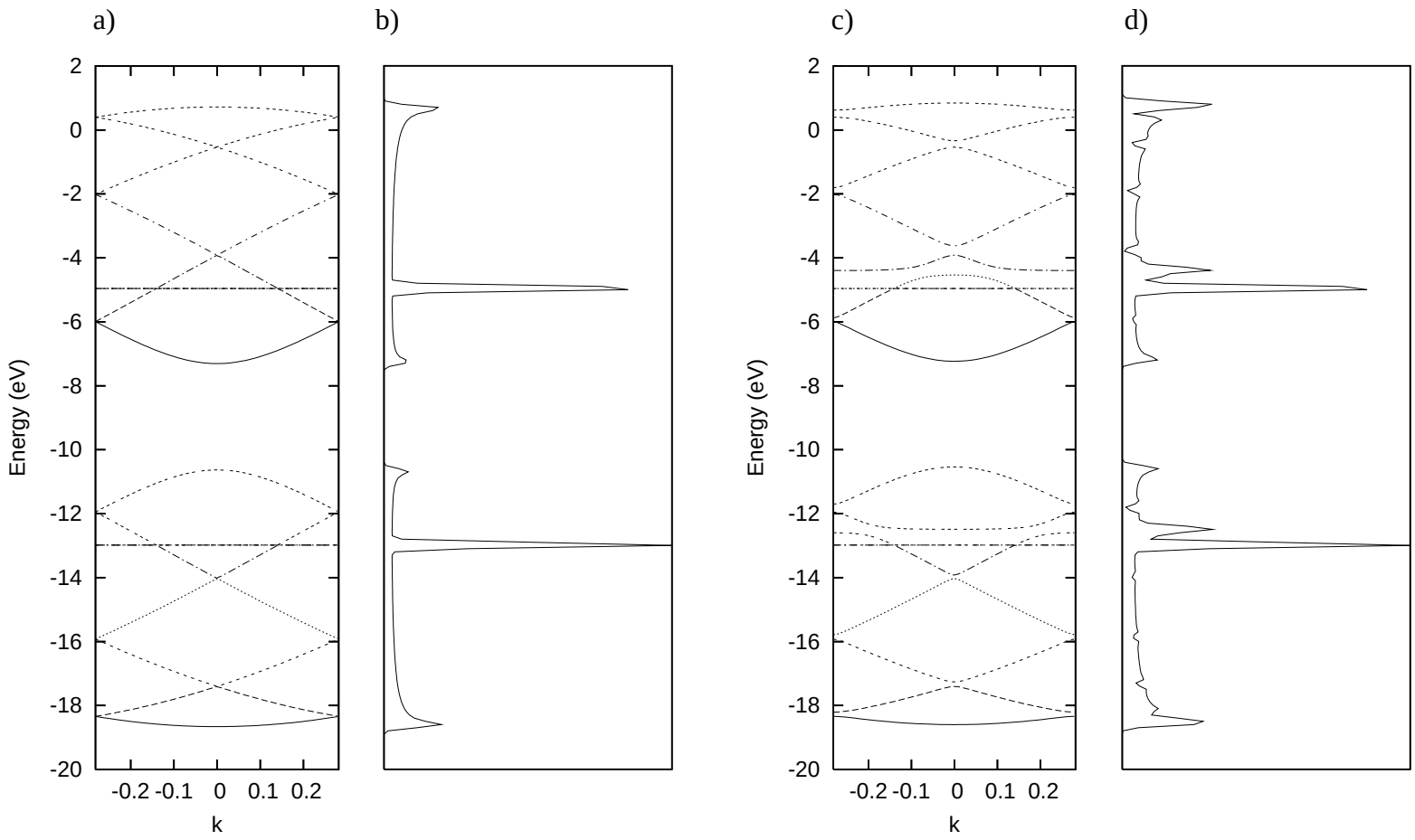

Figure 3.5: Oligophenyl supercell: a) energy bands no perturbation; b) DOS with no perturbation; c) energy bands with 2.0 eV perturbation; d) DOS with 2.0 eV perturbation.

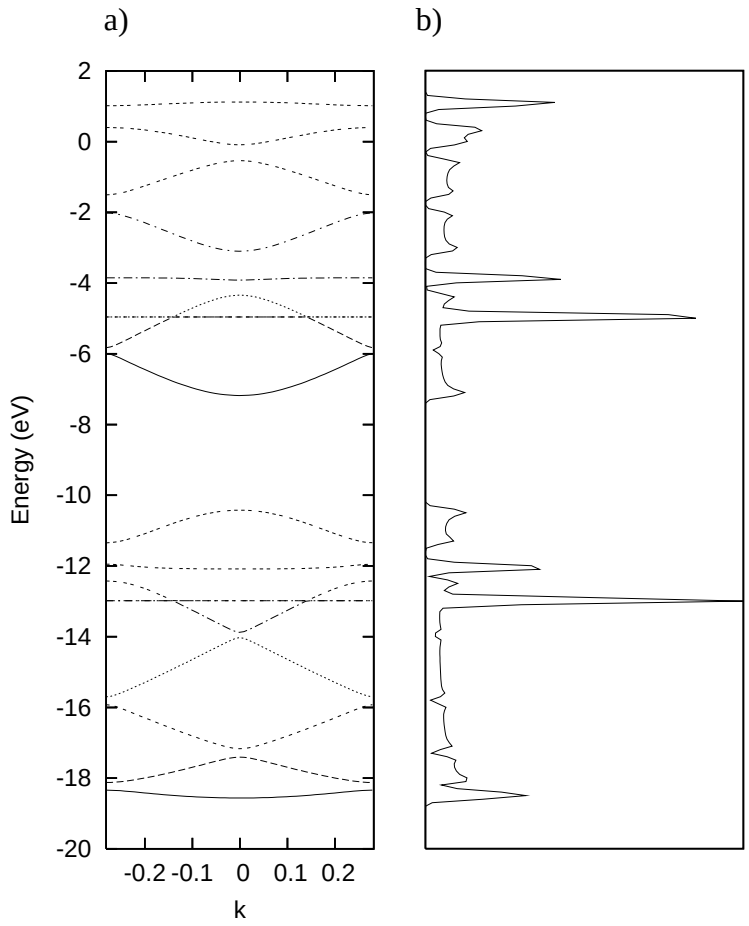

Figure 3.6: The band structure (left) and DOS (right) for the oligophenyl with an edge-atom perturbation of 4.0 eV. A three-phenyl supercell has been used.

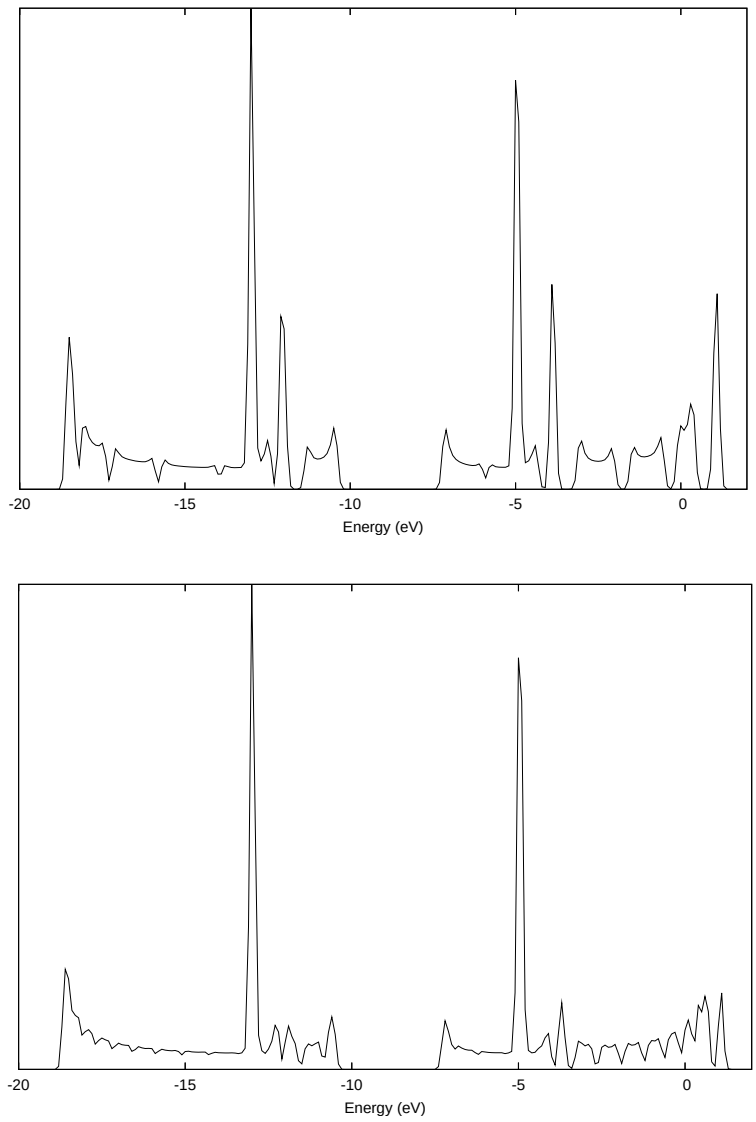

Figure 3.7: The DOS for a three-phenyl ribbon (top) and for a seven-phenyl (bottom). Both DOS have a 4.0 eV on-site edge perturbation. The DOS plots differ as expected in the number of dips caused by the joining of the folded bands at the edges of the Brillioun zone. The number of dips corresponds with the number of times the energy bands are folded—three times in the case of former supercell, and seven in the case of the latter. Additional dips occur at $k_x = 0$ which is also an expected result of a repeating potential.

rather than the wavefunction, $\psi(\vec{r})$, itself. The indices i, k_x indicate the band and wavevector magnitude, respectively. The LDOS is then computationally determined here for only the locations of the atoms of the ribbon as opposed to any location in space, as is possible in the general definition.

For particular values of the LDOS we then isolate specific energies, while performing the sum in Equation 3.3. Figure 3.8 pictorially shows the LDOS for the flat-band energies. The LDOS clearly shows edge states for the flat band, i.e., the density of states is uniformly high for the edge of the ribbon and nearly zero for atoms along the bond axis. The result for the unperturbed case is very similar to the edge states represented by wavefunction coefficients in Figure 3.2. However, the perturbation breaks the symmetry of the system. This is expected because the location of the disorder is on the edge of the phenyl and thus would affect these edge states.

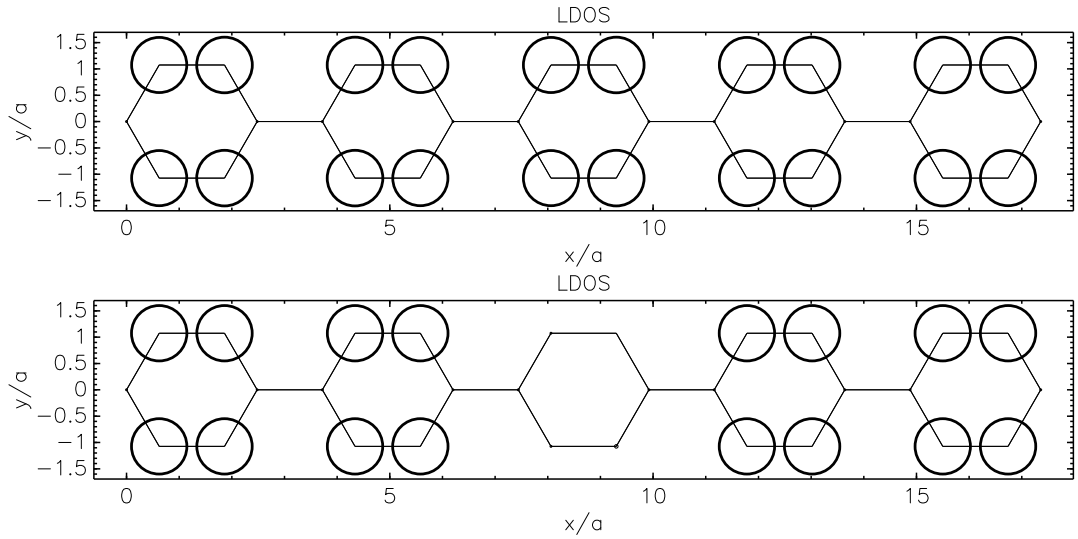

Figure 3.8: The LDOS at -13.0 eV illustrates the edge-state correspondence with the flat energy-bands for the unperturbed case (top) and the edge-perturbed case (bottom).

To further explore the effect of the location of the disorder, it is interesting to view the results of moving the perturbation from a site along the edge to a site on

the bond axis. The resulting DOS and LDOS for a 2.0 eV perturbation to the on-site energy of the next, nearest atom along the bond axis are shown in Figure 3.9. As expected, the LDOS remains unchanged because there is no interaction between the disorder and the atoms along the edge. This is incredibly interesting because given the nearest-neighbor considerations of the tight-binding model, there is (and should be) an interaction between an atom on the phenyl's edge and the atom next to it, along the bond axis. Symmetry considerations disallow this from affecting the DOS. To understand why, it is necessary to recall Figure 3.2. The two edge states both have odd mirror-symmetry. The wavefunction, of course, has this symmetry as well and the odd mirror-symmetry demands that $\psi(0) = 0$ along the bond axis.

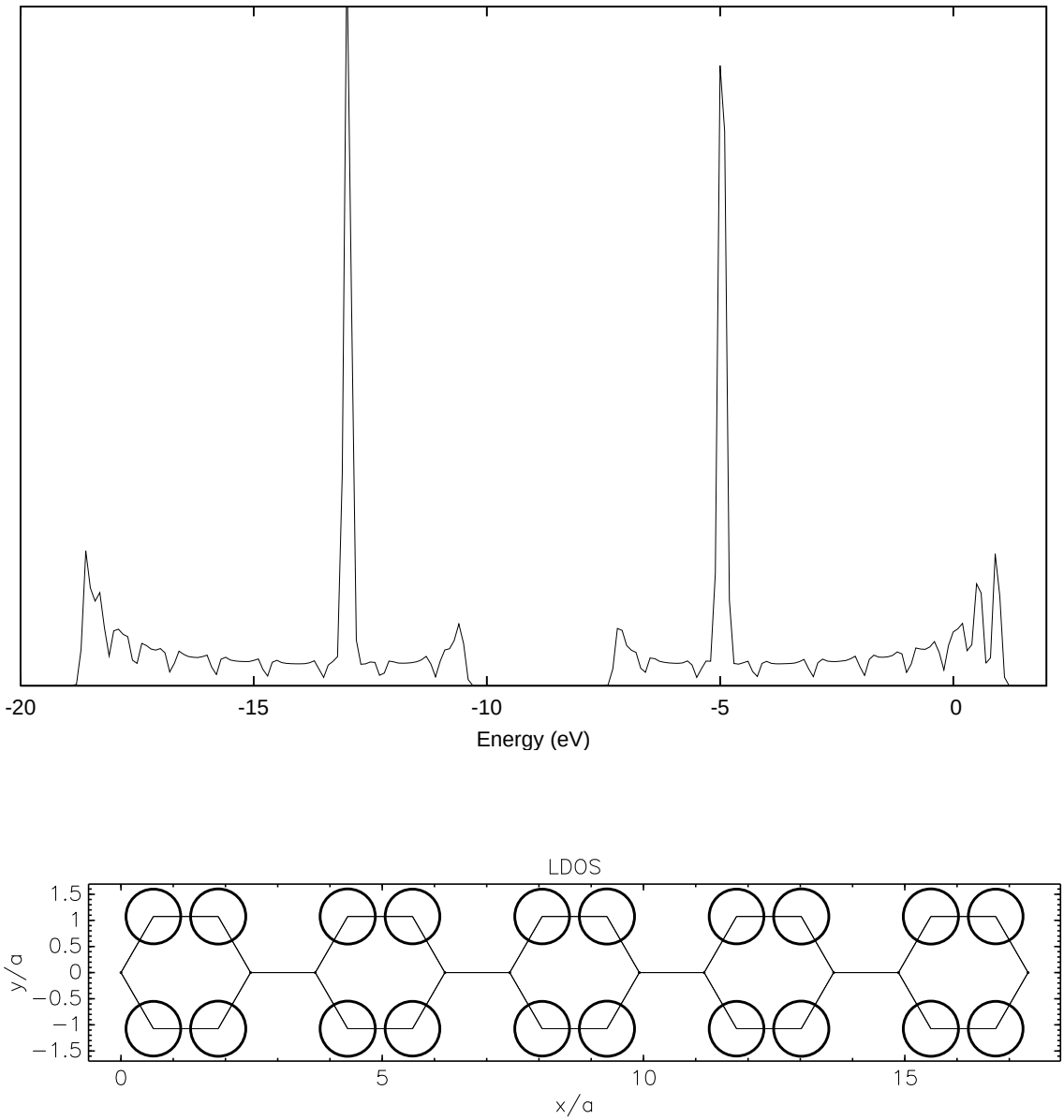

Figure 3.9: The DOS (top) and the LDOS at -13.0 eV (bottom) for a perturbation located along the bond axis. Note that a five-phenyl supercell has been used here.

Chapter 4

Oligoacene

4.1 Unperturbed Oligoacene

4.1.1 Introduction

Chapter 3 applied the tight-binding model to the system of the infinite oligophenyl. In the same spirit, we now investigate the electronic properties of a similar, infinite system—oligoacene. I shall not repeat the details of each step in the proceeding analysis, for the rationale and methods are the same as those discussed at length with the case of the phenyl in the preceding chapter. Albeit, I shall look to identify the interesting features of this system from its electronic structure, both with and without the same type of disorder introduced with the phenyl.

The acene system like the phenyl is an infinite, one-dimensional ribbon composed of carbon hexagons. The oligoacene ribbon has the zigzag edge-structure and is depicted in Figure 4.1. As discussed in Chapter 3 only the p_z-electrons forming π-bonds will be considered in the calculation of the electronic structure.

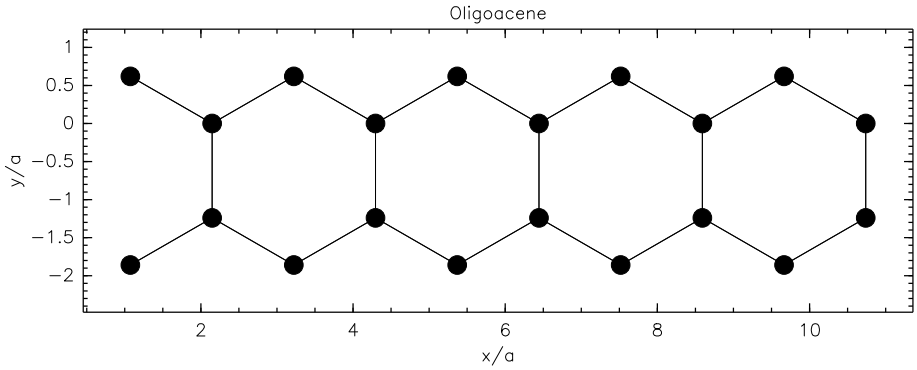

Figure 4.1: Segment of Oligoacene with zigzag edge-structure

4.1.2 Energy and Density of States

The repeating unit-cell chosen for the acene system consists of four carbon atoms, but is slightly more difficult to identify. The cell is depicted in Figure 4.2 with lattice constant $A = a\sqrt{3}$. Applying the form of Equation 2.8 and considering only nearest-

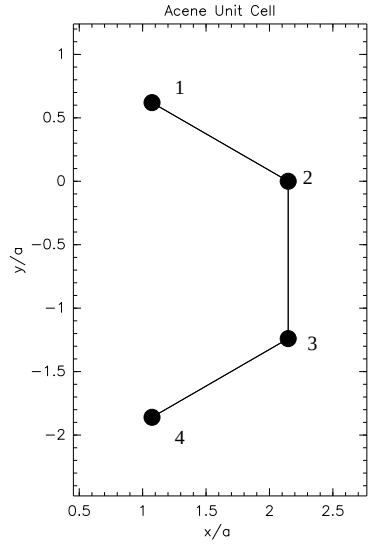

Figure 4.2: The repeating unit-cell for the acene system.

neighbor interactions the resulting Hamiltonian, **H**, where

$$\mathbf{H} = \begin{pmatrix} \epsilon_p & 2V_{pp\pi}\cos k_x a\frac{\sqrt{3}}{2} & 0 & 0 \\ 2V_{pp\pi}\cos k_x a\frac{\sqrt{3}}{2} & \epsilon_p & V_{pp\pi} & 0 \\ 0 & V_{pp\pi} & \epsilon_p & 2V_{pp\pi}\cos k_x a\frac{\sqrt{3}}{2} \\ 0 & 0 & 2V_{pp\pi}\cos k_x a\frac{\sqrt{3}}{2} & \epsilon_p \end{pmatrix}, \tag{4.1}$$

is diagonalized to yield the band structure and DOS shown in Figure 4.3. The Fermi energy, $E_F \approx -9\text{eV}$, is also equal to ϵ_p^c as was the case for the oligophenyl. It is here where the bands touch. The one-dimensional oligoacene appears to have the electronic structure of a metal, as no HOMO-LUMO gap is found. As such, it is useful to investigate perturbative effects to the on-site energy as was done with the case of the oligophenyl. Perhaps such disorder would induce a gap. This scenario is explored in the subsequent section.

The oligoacene also appears to have edge states similar to the phenyl, but the mirror symmetry is even and most importantly, the acene edge-states do not occur at the same energies as the phenyl's edge-states did. For example, Figure 4.4 shows an edge-localization of the electron wavefunction corresponding to the two center bands in Figure 4.3 near energy values of -9.0 eV, the Fermi energy, at the positive X-point. Because these edge states occur at the Fermi energy, they are a remarkable feature and exclusive to zigzag-type nanoribbons. Recall that in Chapter 3 it was found that the oligophenyl system had no such flat bands at the Fermi energy. Thus, these states are extremely interesting because the Fermi energy is located symmetrically between the valence and conduction bands and therefore important for conduction and electron transport.

As in the case of armchair nanoribbons, prior work has investigated these edge

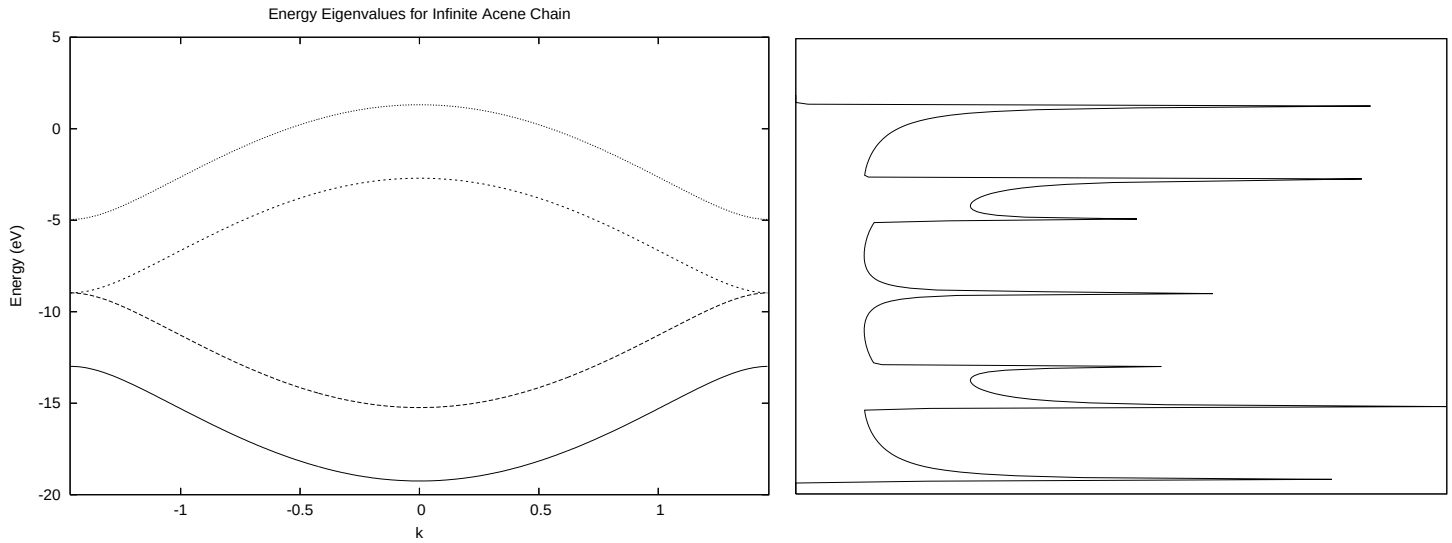

Figure 4.3: a) The band structure for oligoacene. b) DOS for the unperturbed acene system. The unit cell used consists of four carbon atoms. Note $E_F \approx -9.0$ eV.

states at E_F for zigzag ribbons of varying widths [9]. This work on oligoacene confirms these results. As seen in Figure 4.3 the highest valence band and lowest conduction band are degenerate at the X-points and, as noted earlier, correspond to states where charge is localized along the edges of the ribbon which is shown in Figure 4.4. This degeneracy, thus, cannot be a feature of two-dimensional graphene. Other work has shown that the bands possessing this degeneracy become flatter for larger ribbon widths [9, 18].

Our DOS also reflects the unique edge-state of the acene by the presence of the sharp peak at E_F seen in Figure 4.3. In fact, previous investigations have shown that this particular peak is not only to be expected, but diminishes as $1/N$. For example, it has been reported that zigzag ribbons with $N = 51$ (10 nm) demonstrate a non-negligible peak in the DOS [9]. Here, in the limiting oligoacene ($N = 2$) we confirm what therefore should be the largest number of states for a zigzag ribbon of this atomic composition.

4.2 Perturbed Oligoacene

4.2.1 Energy Bands and Density of States

In an analysis similar to the oligophenyl, we study separately the effects of a small perturbation to the on-site energy of a single, carbon atom in the repeating unit-cell. Figure 4.5 shows the locations of the two perturbations. In the first case, the atom nearest the bond axis is perturbed. The unit cell is chosen to be three acenes long with lattice constant, $A = 3a\sqrt{3}$. The corresponding energy and DOS for the case of the perturbation nearest the bond axis are given in Figure 4.6. The most noticeable effect is that of the Bragg scattering which has left significant band-gaps

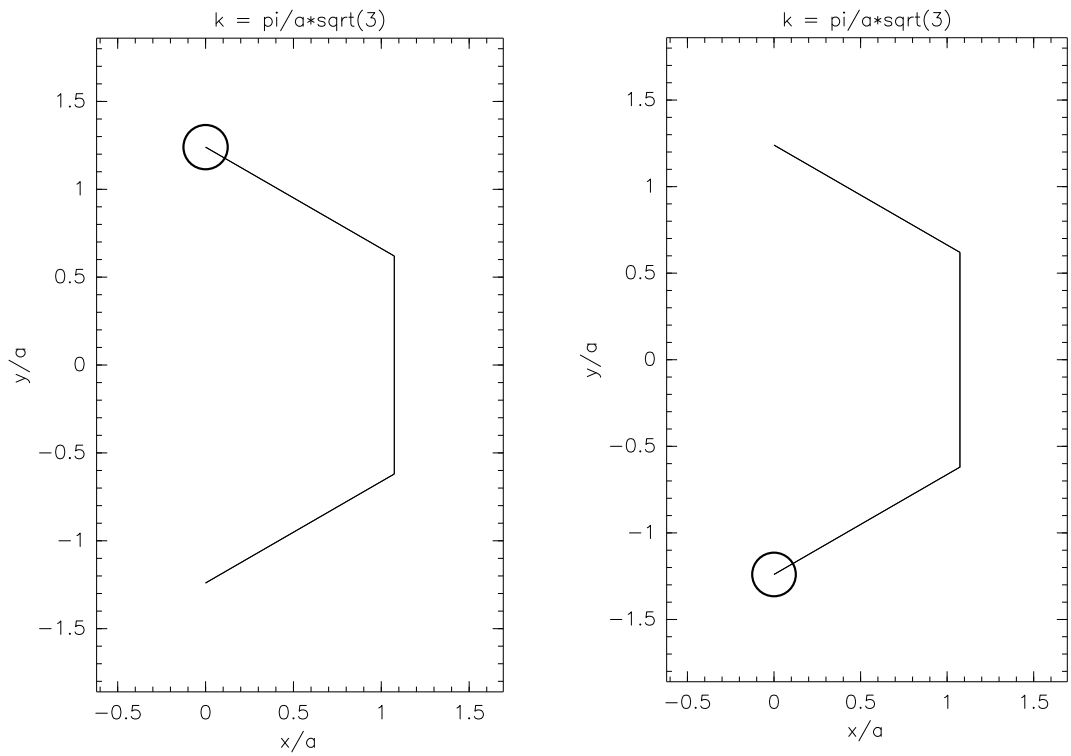

Figure 4.4: Edge states of the unperturbed oligoacene at -9.0 eV at the positive X-point.

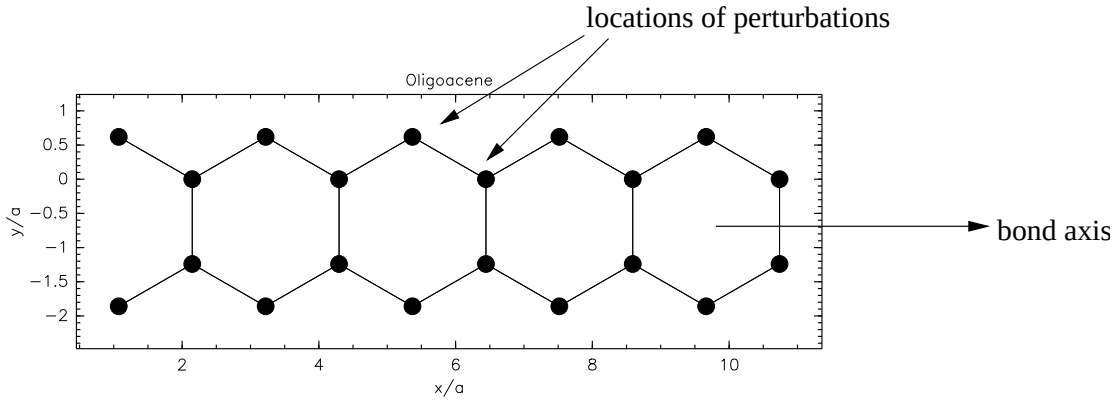

Figure 4.5: The locations for each perturbation. Note that the two cases are studied separately.

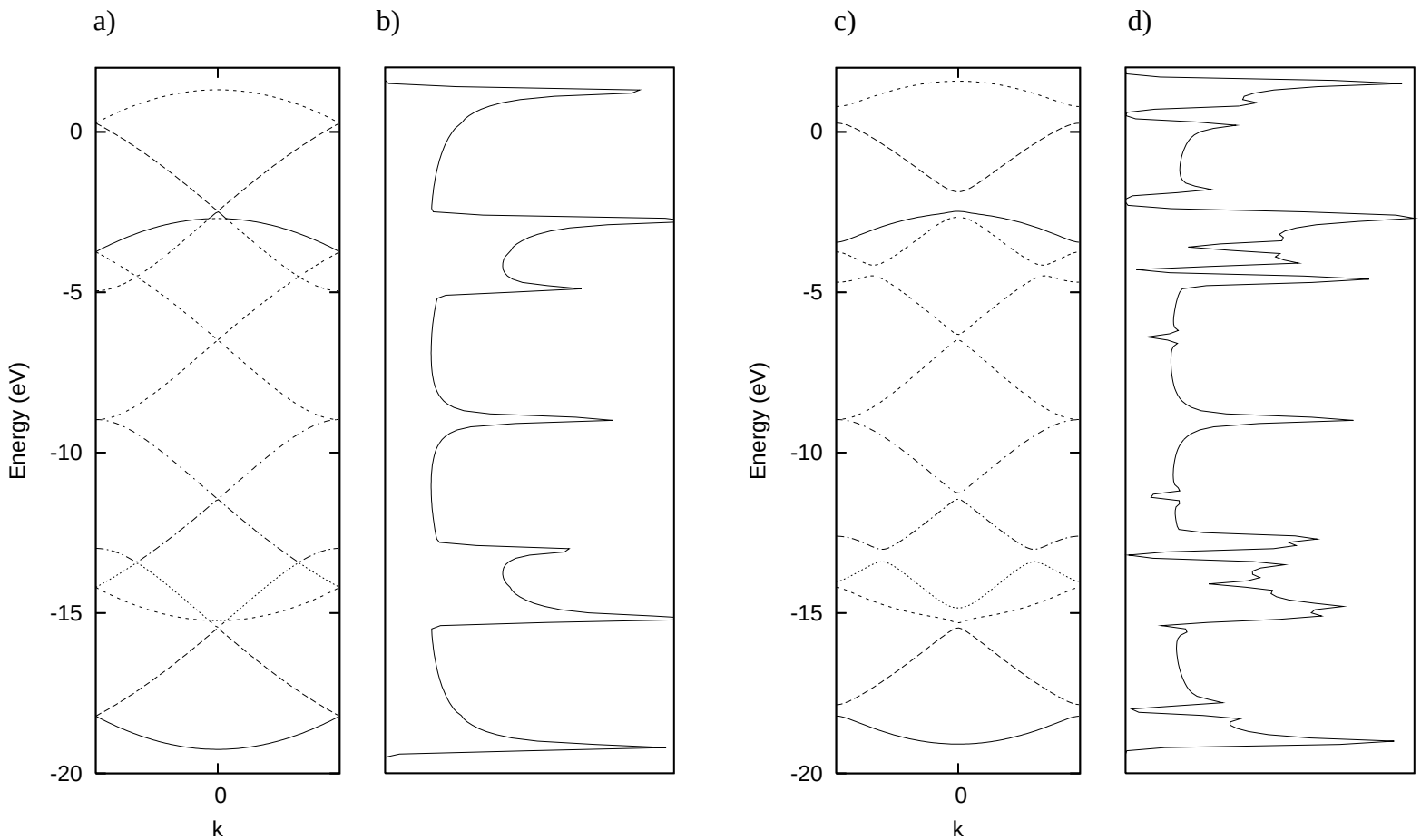

Figure 4.6: a) DOS for unperturbed acene ribbon. b) Energy bands for unperturbed acene ribbon. c) Energy bands for acene ribbon with perturbation nearest the bond axis. d) DOS for acene ribbon with perturbation nearest the bond axis. A three-acene supercell is used and the perturbation is 2.0 eV.

at the edges of the Brillouin zone. Figure 4.6 shows that the largest gaps occur in the conduction bands, such as, between -1 and 1 eV. Apparently, this type of disorder is not an effective means of changing the characterization of the system from a metal to a semiconductor. The effects of Bragg scattering can also be seen from a comparison of the DOS for a three-acene supercell with that of a seven-acene supercell as in Figure 4.7. Both have a 2.0 eV on-site perturbation nearest the bond axis.

The effects of the Bragg scattering increase the number of dips in the DOS due to the greater number of band-foldings. For instance, within the region of -15 to -20 eV, the frequency of the dips increases significantly from the three-acene supercell to that of the seven. There seems to be fewer interesting features from the disorder here than in the case of the phenyl. What does remain is the overall asymmetry between the valence and conduction bands when the disorder is introduced. There are wider gaps at the zone edges as well as a compression of the energy structure in the conduction bands verses the valence.

4.2.2 LDOS

As was the case with the oligophenyl ribbon, the degeneracy at the X-points of the HOMO-LUMO gap is also unaffected by the disorder. This is expected because these are edge states and the perturbation has been introduced near the bond axis as opposed to the edge. When the 2.0 eV on-site energy-perturbation is shifted to the edge of the acene ribbon, the symmetry of the edge states is no longer preserved. This effect is captured well in the LDOS. Figure 4.8 contrasts the LDOS and edge states pictorially, for each location of the perturbation. When the non-edge atom is perturbed, the LDOS at -9.0 eV remains unchanged relative to the unperturbed system, so that the localization of charged is symmetric on the ribbon's edge atoms.

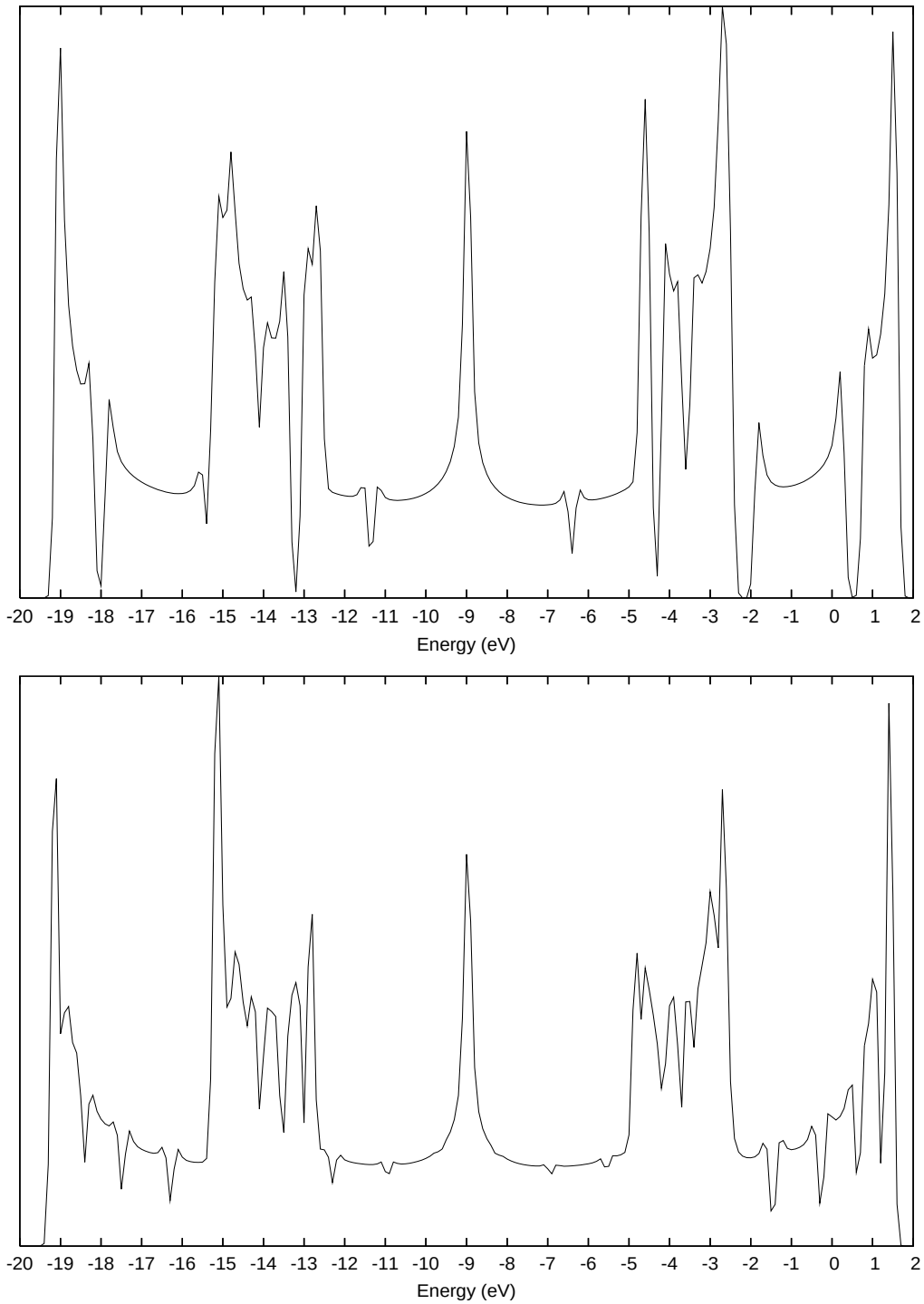

Figure 4.7: DOS for three-acene supercell (bottom) and seven-acene supercell (top). The perturbation is 2.0 eV.

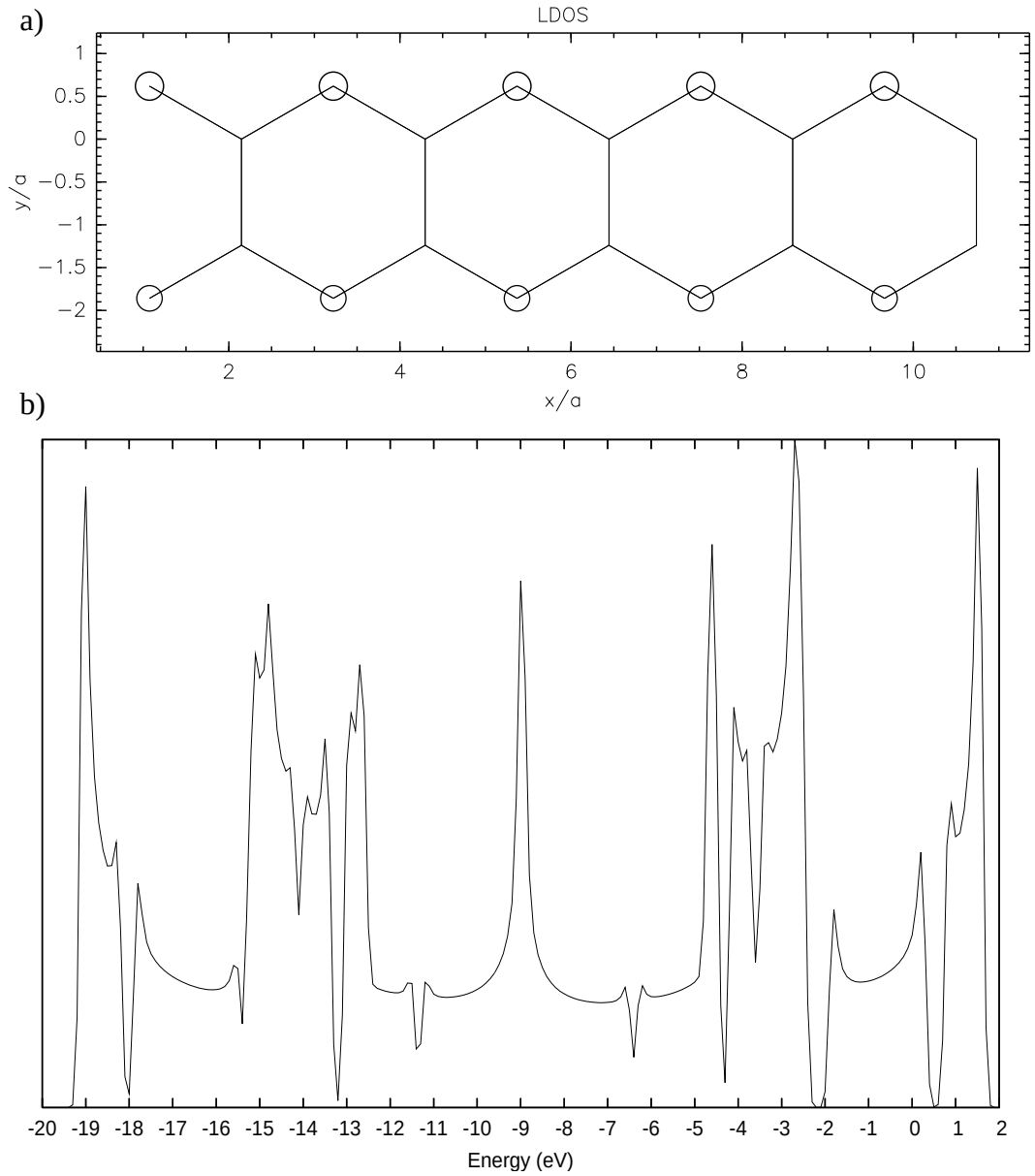

Figure 4.8: a) LDOS at -9.0 eV for the perturbation nearest the bond axis; b) DOS for perturbation nearest bond axis.

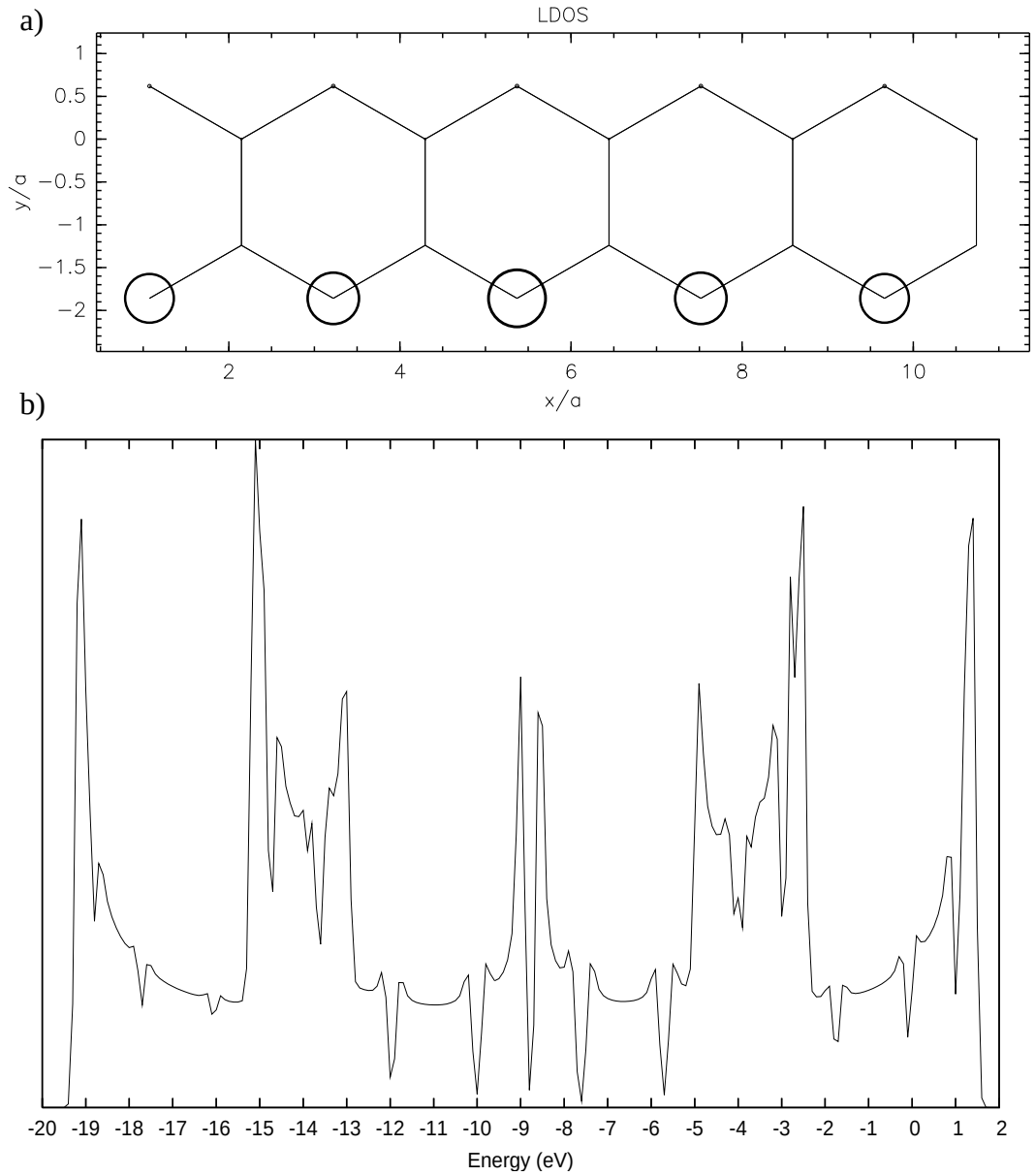

Figure 4.9: a) LDOS at -9.0 eV for the perturbation on the edge; b) DOS for the edge perturbation.

This feature is due to the fact that the disorder is not on the edge. More importantly is the feature that an electron wave at the edge of the Brillouin zone with wavevector, $k_x = \pm\pi/A$, is a standing wave and has antinodes on the edge-atom positions. This then forces the amplitude of the wave to have nodes at the positions of the central atoms, forming nodal planes there. Hence, for the edge states of the acene, which occur at $k_x = \pm\pi/A$, this particular wave-phenomenon is expected. When the edge atom is perturbed the LDOS no longer respects the symmetry of equal charge on the edges. And more charge is localized near the bottom edge of the ribbon.

As can be seen from Figure 4.8 and Figure 4.9, it appears that the edge perturbation has the effect of splitting the sharp peak in the DOS at -9.0 eV into two less-broad peaks. As a result this edge perturbation has enduced a slight, non-zero HOMO-LUMO gap, the size of which is proportional to the splitting energy. The new gap has lifted the Fermi-energy degeneracy which was present in the prior cases. Figure 4.9 shows the LDOS for the new peak of lower energy, i.e, at -9.0 eV., where most of the charge concentrates on the bottom edge of the ribbon. It is reasonable, then, to expect that the LDOS for the new, higher-energy peak at -8.5 eV would correspond to a similar state where charge is primarily localized along the top of the ribbon. Indeed, this is the result as Figure 4.10 shows.

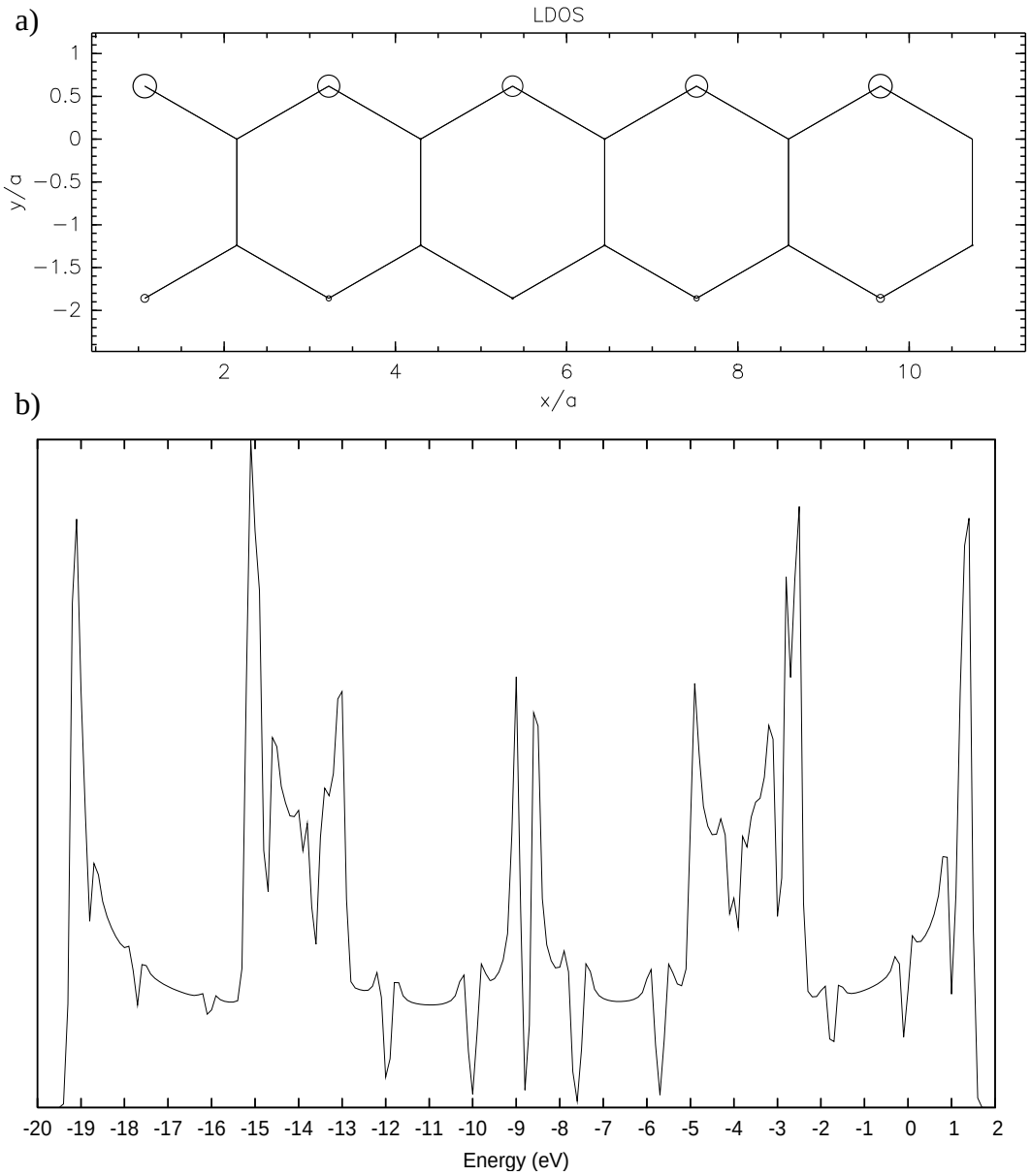

Figure 4.10: a) LDOS at -8.5 eV for a 2.0 eV edge perturbation; b) DOS for the edge perturbation.

Chapter 5

Summary and Conclusions

This work has examined two, idealized nanoscale systems—oligophenyl and oligoacene in their limiting cases of infinite length. As the first study of its kind for us, much of the resulting productivity has focused on the development of the basic machinery necessary to model the electronic structure of the systems. Although it was not the focus of this work, much time was spent developing the computational tools necessary for all calculations. Examples of these have been included in the Appendices.

A theoretical analysis using the tight-binding technique has been used with the goal of quickly identifying interesting features which have contributed to the enormous popularity of these and similar nanostructures. The proceeding commentary briefly reviews what interesting results this work has determined about each of these systems and prognosticates on possible, future avenues of study.

The tight-binding model was first introduced in Chapter 2 along with its advantages, limitations, and its mathematical prescription. The electronic structures of oligophenyl and oligoacene were then determined using a single unit-cell and implementing periodic boundary-conditions. From these data the density of states and local density of states were calculated and discussed in detail in Chapters 3 and 4. Each

system was found to have unique, electron-positron symmetry as well as important localized-states. Disorder was then introduced into each system at two distinct locations on each ribbon using an expanded supercell. The disorder negligibly narrowed the band gap as well as flattened certain energy-bands. Most interesting however, was the symmetry breaking due to the perturbations.

The oligophenyl was found to have the electronic structure of a semiconductor. It was also found to have flat bands which corresponded to particle states of infinite mass where charge was exclusively localized along the edges. Because of this feature, they would not allow conduction along the bond axis. These states also had wavefunction coefficients which exhibited odd mirror-symmetry, the importance of which seems nebulous until one considers this symmetry as necessary to explain the unexpected results of the differing placements of the perturbation. That is to say, when the perturbation was moved from an edge atom to an atom along the bond axis, nearest-neighbor considerations would still predict that the resulting disorder would influence the resulting states. However, this was not found to be the case. The mirror symmetry embedded in the Hamiltonian presents itself on the system and therefore forces no charge to be localized along the bond axis.

The metallic, oligoacene also exhibited symmetries such as the splitting of the large, center peak in the DOS in the presence of an edge-atom perturbation. Very interestingly the peak was separated into two sharper peaks, one of which was shifted to a slightly higher energy. At present, the symmetry mechanism of this feature has not been identified. Like the oligophenyl the acene has the wavefunction symmetry that forces charge localization along the bond axis to terminate even in the presence of both placements of perturbations. All of these features rely heavily upon the symmetry of the tight-binding Hamiltonian, in fact, so much so that there is a substantial basis to conclude that a detailed and reflective understanding of the symmetries of

each of these systems would be most helpful in the prediction of the systems' complete electronic-structures.

Both the one-dimensional oligoacene and oligophenyl have exhibited localized states, i.e. the edge states resulting from the large peaks in the DOS. These states reflect the concentration of charge along the edges of the ribbon. It is known that the breakage of the translational symmetry of a lattice in certain directions, causes such states. When graphitic sheets are cut they subsequently lack the two-dimensional periodic boundary-conditions and the resulting, C-dangling bonds lead to these localized states at the Fermi energy [18] and other energies where the DOS peaks. This work has confirmed that such states do exist in the limiting cases of extreme, one-dimensional oligophenyl and oligoacene. In particular, this work is interesting because it illuminates such an extreme version of GNRs, and as a result demonstrates features which become less distinct in the cases of finite ribbons with larger, more realistic widths where the corresponding electronic structures seem to more closely mimic that of two-dimensional graphene [9].

Much work as been done to investigate the effects of types of disorder other than the on-site energy perturbations which have been performed here. The author would find it interesting to examine the effects of random, on-site perturbations to these same systems which would more closely mimic the limit of physically realizable oligophenyl and oligoacene ribbons. Random, isovalent doping, would also be interesting to investigate. Most immediately, the effect of introducing random, C-atoms along the edges of the ribbons should be studied in any extension of this work.

Appendix A

Sample Python Codes

A.1 Scripting for Generating the Hamiltonian

```
__author__ = "Adam Hinkle"
__version__ = 1.0

## This script generates a Hamiltonian for a 1-D nanoribbon using the tight-
## model. The list of variables ("N" through "k") below must be given values in
## any script where this script has been imported.


import numpy
import scipy.linalg
import scipy

##N = number of atoms
##A               = lattice constant
##a               = C-C bond length (in Angstroms)
##atompostions    = array of atoms coordinates
##e               = onsite energy (in eV)
##V               = overlap energy (in eV)
##U               = array for location of impurity or perturbation value
##k               = magnitude of wavevector

def Hinkletonian(N,A,a,atompositions,e,V,U,k):
    h=numpy.zeros((N,N),dtype=complex)

    for i in range(N):
        h[i,i]= e + U[i]

    for i in range(N):

        for j in range(N):

            for I in range(-1,2,1):

                xi=atompositions[i,0]
                xj=atompositions[j,0]
                yi=atompositions[i,1]
                yj=atompositions[j,1]

                x=xi-xj-I*A
                y=yi-yj
                r=numpy.sqrt(x*x+y*y)

                if numpy.abs(r-a) < 0.000001:

                    h[i,j]=h[i,j]+V*numpy.exp(1.0j*k*x)

    eigenvalues, eigenvectors = scipy.linalg.eigh(h)

    return eigenvalues, eigenvectors
```

A.2 Density of States

```
import numpy
import scipy.linalg
import scipy

# This script calculates the density of states for a 1-D nanoribbon. You must
# input the coordinates of the atoms in "atompositions" array. Note to set
# variables "KT through D" (below) for your particular ribbon and supercell.

# common declarations
pi=numpy.pi
exp=numpy.exp
sqrt=numpy.sqrt



#define two empty arrays to store the independent energy values and the eigenvalues
EList = numpy.array([])
biglist = numpy.array([])


#import Hinkletonian into file here from hamiltonian.py
import hamiltonian


KT=0.1                  # imput value of KT
e=-8.97                 # carbon on-site energy
V=-4.0142               # overlap parameter
a=1.24                  # carbon-carbon bond length
A=15*a                  # lattice constant
N=30                    # no. of atoms per repeating cell
D=pi/(1000*A)           # increment of for-loop of k

# used in atompositions
f=numpy.sqrt(3.0)/2
g=0.5
atompositions=numpy.array( ( \
(3*g*a,f*a),(2*a,0),(3*g*a,-f*a),(g*a,-f*a),(0,0),(g*a,f*a),\
(3*g*a+3*a,f*a),(2*a+3*a,0),(3*g*a+3*a,-f*a),(g*a+3*a,-f*a),(0+3*a,0),(g*a+3*a,f*a),\
(3*g*a+6*a,f*a), (2*a+6*a,0), (3*g*a+6*a,-f*a),(g*a+6*a,-f*a), (0+6*a,0), (g*a+6*a,f*a),\
(3*g*a+12*a,f*a),(2*a+12*a,0),(3*g*a+12*a,-f*a),(g*a+12*a,-f*a),(0+12*a,0),(g*a+12*a,f*a),\
(3*g*a+24*a,f*a),(2*a+24*a,0),(3*g*a+24*a,-f*a),(g*a+24*a,-f*a),(0+24*a,0),(g*a+24*a,f*a)\
) )


# array for IMPURITY
U=numpy.array((0,0,0,0,0,0,0,0,0,0,0,0,0,2.0,0,0,0,0,0,0,0,0,0,0,0,0,0,0,0,0,0))
```

```
# for loop used to diagonalize Hamiltonian and return and store energy-eigenvalues
# the range used in the for-loop avoids points of symmetry in equally spaced
increments
#of k. This construction will necessitate the DOS to be doubled at the end because
here
#we only include positive values of k
for k in numpy.arange(D/2,(pi/A)+(D/2),D):

    evalues, evectors = hamiltonian.Hinkletonian(N,A,a,atompositions,e,V,U,k)

    biglist = numpy.concatenate( (biglist, evalues))


#Generate independent list of energy values, E. and store in an array called EList.
EList = numpy.arange(-25.0,10.0,0.1)


##now we evaluate the gaussian sum which is a function of E
#but also depends on E_i. The gaussian is also normalised.
for E in EList:

    sum = 0

    for eigenvalue in biglist:
        b = numpy.exp(      -( (1/(KT))*(E - eigenvalue))**2 )
        sum = sum + b*( (1/sqrt(pi*2)) * (1/(KT)) )

    print E, 2.0*(D/(2*pi))*sum
## this gives one data point : (E, D(E) ). however, when the first loop is done
    #there will be a list of these points.
```

A.3 Local Density of States

```
import numpy
import scipy.linalg
import scipy
"""Author: Adam Hinkle

This script calculates the LDOS for a 1-D nanoribbon. You must modify/include
the atompositions below as well as check and modify the parameters "KT" through
"E". You must modify/set the arguments of the "p=plottbdensity" function. Note
that the structure is quite similar to the DOS script which is subsumed in this
calculation"""

# common declarations
pi=numpy.pi
exp=numpy.exp
sqrt=numpy.sqrt

#import Hinkletonian into file here from hamitonian.py
import hamiltonian


KT=0.1                  # imput value of KT
e=-8.97                 # carbon on-site energy
V=-4.0142               # overlap parameter
a=1.24                  # carbon-carbon bond length
A=15*a                  # lattice constant
N=30                    # rank of square matrix (Hamiltonian)
L=3                     # no. of nearest-neighbor cells
D=pi/(1000*A)           # increment of for-loop of k
E=-13.0                 # Energy of interest (in eV)


# used in atompositions
f=numpy.sqrt(3.0)/2
g=0.5
s=2*f
atompositions=numpy.array( (
(3*g*a,f*a),(2*a,0),(3*g*a,-f*a),(g*a,-f*a),(0,0),(g*a,f*a),\
(3*g*a+3*a,f*a),(2*a+3*a,0),(3*g*a+3*a,-f*a),(g*a+3*a,-f*a),(0+3*a,0),(g*a+3*a,f*a),\
(3*g*a+6*a,f*a),(2*a+6*a,0),(3*g*a+6*a,-f*a),(g*a+6*a,-f*a),(0+6*a,0),(g*a+6*a,f*a),\
(3*g*a+9*a,f*a),(2*a+9*a,0),(3*g*a+9*a,-f*a),(g*a+9*a,-f*a),(0+9*a,0),(g*a+9*a,f*a),\
(3*g*a+12*a,f*a),(2*a+12*a,0),(3*g*a+12*a,-f*a),(g*a+12*a,-f*a),(0+12*a,0),(g*a+12*a,f*a)\
) )

# array for IMPURITY
U=numpy.array((0,0,0,0,0,0,0,0,0,0,0,0,0,2.0,0,0,0,0,0,0,0,0,0,0,0,0,0,0,0,0,0))
```

```
#The plotting script is imported from the file plotdensity.py. For a single
#value of k the N eigenvalues and eigenvectors are obtained in the first for
#loop and then called up in the second loop and the DOS/LDOS is calculated.
#There is a normalisation factor of 1/sqrt(L*N).

LDOS = 0

from plottbdensity import plottbdensity

for k in numpy.arange(D/2,(pi/A)+(D/2),D):

    evalues, evectors = hamiltonian.Hinkletonian(N,A,a,atompositions,e,V,U,k)

    for i in range(N):
      eigenvalue = evalues[i]
      eigenvector = evectors[:,i]
        DOS = numpy.exp(      -( ((1/(KT))**2)*(E - eigenvalue))**2 )
*(1/(L*N*sqrt(pi*KT)))


        prob = eigenvector*numpy.conjugate(eigenvector)

        LDOS = LDOS + DOS*prob

#command to make plots of LDOS on the atompositions
p = plottbdensity(atompositions,LDOS,a,dotsize=50.0,plottitle="LDOS", \
                      output="EPS", plotfile="LDOSphenylcenter")
```

Appendix B

Additional Matrix-Hamiltonian Scripts

```
import numpy
import scipy.linalg
import scipy

"""Author: Adam Hinkle

This script returns the energy eigenvalues and eigenvectors of the
Hamiltonian for the oligophenyl using a three-phenyl supercell. The method is
simple but has been replaced by the more general script described in Appendix A1
which works for any 1-D nanoribbon. Read over the variables below and modify as
as needed"""

# common declarations
pi=numpy.pi
exp=numpy.exp

e=-8.97             #on-site energy (eV)
v=-4.0142           #overlap parameter
a=1.24              #carbon-carbon bond length
I=0.0               #perturbation strength of one atom in matrix below


for k in numpy.arange((-pi/(9*a)),(pi/(9*a)),0.01):

    h=numpy.matrix( [[e,v*exp(k*0.62j),0,0,0,v*exp(-k*1.24j),0,0,0,0,0,0,0,0,0,0,0,0],\
        [v*exp(-k*0.62j),e,v*exp(-k*0.62j),0,0,0,0,0,0,0,v*exp(k*1.24j),0,0,0,0,0,0,0],\
        [0,v*exp(k*0.62j),e,v*exp(-k*1.24j),0,0,0,0,0,0,0,0,0,0,0,0,0,0],\
        [0,0,v*exp(k*1.24j),e,v*exp(-k*0.62j),0,0,0,0,0,0,0,0,0,0,0,0,0],\
        [0,0,0,v*exp(k*0.62j),e,v*exp(k*0.62j),0,0,0,0,0,0,0,v*exp(-k*1.24j),0,0,0,0],\
        [v*exp(k*1.24j),0,0,0,v*exp(-k*0.62j),e,0,0,0,0,0,0,0,0,0,0,0,0],\
        [0,0,0,0,0,0,e+I,v*exp(k*0.62j),0,0,0,v*exp(-k*1.24j),0,0,0,0,0,0],\
        [0,0,0,0,0,0,v*exp(-k*0.62j),e,v*exp(-k*0.62j),0,0,0,0,0,0,0,v*exp(k*1.24j),0],\
        [0,0,0,0,0,0, 0,v*exp(k*0.62j),e,v*exp(-k*1.24j),0,0,0,0,0,0,0,0],\
        [0,0,0,0,0,0,0,0,v*exp(k*1.24j),e,v*exp(-k*0.62j),0,0,0,0,0,0,0],\
        [0,v*exp(-k*1.24j),0,0,0,0,0,0,0,v*exp(k*0.62j),e,v*exp(k*0.62j),0,0,0,0,0,0],\
        [0,0,0,0,0,0,v*exp(k*1.24j),0,0,0,v*exp(-k*0.62j),e,0,0,0,0,0,0],\
        [0,0,0,0,0,0,0,0,0,0,0,0,e,v*exp(k*0.62j),0,0,0,v*exp(-k*1.24j)],\
        [0,0,0,0,v*exp(k*1.24j),0,0,0,0,0,0,0,v*exp(-k*0.62j),e,v*exp(-k*0.62j),0,0,0],\
        [0,0,0,0,0,0,0,0,0,0,0,0,0,v*exp(k*0.62j),e,v*exp(-k*1.24j),0,0],\
        [0,0,0,0,0,0,0,0,0,0,0,0,0,0,v*exp(k*1.24j),e,v*exp(-k*0.62j),0],\
        [0,0,0,0,0,0,0,v*exp(-k*1.24j),0,0,0,0,0,0,0,v*exp(k*0.62j),e,v*exp(k*0.62j)],\
        [0,0,0,0,0,0,0,0,0,0,0,0,v*exp(k*1.24j),0,0,0,v*exp(-k*0.62j),e]] )


    eigenvalues, eigenvectors = scipy.linalg.eigh(h)

    print k, eigenvalues[0], eigenvalues[1], eigenvalues[2], eigenvalues[3],\
          eigenvalues[4], eigenvalues[5], eigenvalues[6],\
          eigenvalues[7], eigenvalues[8], eigenvalues[9], eigenvalues[10],\
          eigenvalues[11], eigenvalues[12], eigenvalues[13],\
          eigenvalues[14], eigenvalues[15], eigenvalues[16],\
          eigenvalues[17]
```

Bibliography

[1] Mildred Dresselhaus. "From graphene to graphite to nanotubes to graphene—2008 March Meeting of the APS, tutorial on graphene." URL `http://www.physics.gatech.edu/npeg/publications/APS_08Graphene_Tutorial_Dresselhaus.pdf`.

[2] Jean-Christophe Charlier, Xavier Blase, and Stephen Roche. *Rev. Mod. Phys.* **79**, 667 (2007).

[3] K.S. Novoselov, D. Jiang, F. Schedin, T. Booth, V. Khotevich, S. Morozov, and A. Geim. *PNAS* **102**, 10451 (2005).

[4] J. Hass, R. Feng, T. Li, X. Li, Z. Zong, W. A. de Heer, P. N. First, E. H. Conrad, C.A. Jeffery, and C. Berger. *Appl. Phys. Lett.* **89**, 143106 (2006).

[5] S. Iijima. *Nature* **354**, 56 (1991).

[6] Paul L. McEuen, Michael S. Fuhrer, and Hongkun Park. *IEEE Transactions on Nanotechnology* **1**, 78 (2002).

[7] J. X. Cao, X. H. Yan, J. W. Ding, and D. L. Wang. *J. Phys.: Condensed Matter* **13**, L271 (2001).

[8] Philip Shemella, Y. Zhang, M. Mailman, P. M. Ajayan, and S. Nayak. *Appl. Phys. Lett.* **91**, 042101 (2007).

[9] K. Nakada, M. Fujita, G. Dresselhaus, and M.S. Dresselhaus. *Phys. Rev. B* **54**, 17954 (1996).

[10] Denis A. Areshkin, Daniel Gunlycke, and Carter T. White. *Nano Lett.* **7**, 204 (2007).

[11] Richard M. Martin. *Electronic Structure: Basic Theory and Practical Methods.* Cambridge University Press (2004).

[12] Walter A. Harrison. *Electronic Structure and the Properties of Solids: The Physics of the Chemical Bond.* Dover (1989).

[13] National Institute for Standards and Technology (NIST). "Computational chemistry comparison and benchmark database." URL `http://cccbdb.nist.gov`.

[14] M. Fujita, K. Wakabayashi, and K. Kusakabe. *J. Phys. Soc. Jpn.* **65**, 1920 (1996).

[15] S.E. Stein and R. L. Brown. *J. Am. Chem. Soc.* **109**, 3721 (1987).

[16] K. Tanaka, S. Yamashita, H. Yamabe, and T. Yamabe. *Synth. Met.* **17**, 143 (1987).

[17] M. Fujita, M. Yoshida, and K. Nakada. *Fullerene Sci. Technol.* **4**, 565 (1996).

[18] Yoshiyuki Miyamoto, Kyoko Nakada, and Mitsutaka Fujita. *Phys. Rev. B* **59**, 9858 (1999).